210Po and 210Pb distribution,dissolved-particulate exchangerates, and particulate export along the North Atlantic US GEOTRACES GA03 section

Sylvain Rigaud, Gillian Stewart, Mark Baskaran, D Marsan, Thomas Church

Deep-Sea Research II ∎ (∎∎∎∎) ∎∎∎–∎∎∎

Contents lists available at ScienceDirect

Deep-Sea Research II

journal homepage: www.elsevier.com/locate/dsr2

^{210}Po and ^{210}Pb distribution, dissolved-particulate exchange rates, and particulate export along the North Atlantic US GEOTRACES GA03 section

S. Rigaud [a,*], G. Stewart [b], M. Baskaran [c], D. Marsan [a], T. Church [a]

[a] School of Marine Science and Policy, University of Delaware, Newark, DE 19716, USA
[b] School of Earth and Environmental Sciences, Queens College CUNY, Flushing, NY 11367-1575, USA
[c] Department of Geology, Wayne State University, Detroit, MI 48202-3622, USA

ARTICLE INFO

Keywords:
^{210}Po
^{210}Pb
North Atlantic Ocean
Hydrothermal plume
Benthic nepheloid layer
GEOTRACES

ABSTRACT

Vertical profiles of ^{210}Po and ^{210}Pb in the water column were measured in the dissolved phase (<0.45 μm), and small (0.8–51 μm) and large (>51 μm) particles at seven stations along the US GEOTRACES North Atlantic Zonal Transect (GA03). Mass balance calculations were employed to assess nuclide exchange rates at the dissolved-small particle interface and between small and large particles, and to quantify export with settling large particles. In the surface ocean, ^{210}Po scavenging is linearly correlated with the concentration of particulate organic carbon (POC) in large particles, supporting the role of biogenic particle in ^{210}Po bioaccumulation and export. In stations near the coast, this link is more complex due to the variable source of biogenic material and temporal changes in the surface biogeochemical and physical conditions. At depth, ^{210}Po exhibits significant widespread deficit with respect to ^{210}Pb that could in part be attributed to in situ ^{210}Po scavenging and may be related to surface biological productivity. As previously reported the ^{210}Pb scavenging rates in the surface ocean were higher at ocean margins. At depth, ^{210}Pb scavenging increases with depth and eastward due to the increase of adsorption sites available in the benthic layers and to a regional contribution of benthic ^{210}Pb scavenging and/or particle flux, respectively. The benthic nepheloid layer (BNL) and the Hydrothermal TAG plume distinctly enhance ^{210}Pb scavenging due to increased surface adsorption in association with resuspended or freshly formed particles. In contrast, ^{210}Po is not seen to be significantly scavenged in these environments due to its relatively short half-life and the long residence time of particles.

1. Introduction

Trace element biogeochemistry in the ocean has an important control on marine ecosystem functioning and the carbon cycle. The naturally occurring ^{210}Po ($T_{1/2}$=138.4 d) and ^{210}Pb ($T_{1/2}$=22.3 y) radionuclides have been widely used to examine dissolved and particle dynamics in marine ecosystems over the past several decades (e.g., Bacon et al., 1976; Nozaki et al., 1976; Thomson and Turekian, 1976; Cochran, 1992; Cochran and Masque, 2003; Rutgers van der Loeff and Geibert 2008). Both nuclides are part of the ^{238}U decay chain, with ^{210}Pb being produced from the decay of ^{226}Ra ($T_{1/2}$=1601 y) via several short lived radionuclides (^{222}Rn, ^{218}Po, ^{214}Pb, ^{214}Bi, ^{214}Po; ^{222}Rn $T_{1/2}$=3.8 d; others less than 30 min) while ^{210}Po is produced from the decay of ^{210}Pb via ^{210}Bi ($T_{1/2}$=5.0 d). In seawater, ^{226}Ra exhibits mainly conservative behavior while both ^{210}Pb and ^{210}Po are surface particle reactive, but ^{210}Po also bioaccumulates within organic tissues (Heyraud and Cherry, 1979; Stewart and Fisher, 2003a, 2003b; Stewart et al., 2005). As such, differences in the specific activity between ^{210}Pb and ^{226}Ra and between ^{210}Po and ^{210}Pb in the water column can be used to quantitatively assess dissolved-particulate exchange rates and export fluxes of sinking particulate material over time scale of months (^{210}Po) and decades (^{210}Pb). Such rates can then be applied to the understanding of biogeochemical cycles of other trace elements that display similar bioactive or particle reactive chemical behavior. Among the most common applications of such tracers are the use of ^{210}Pb disequilibrium to assess scavenging rates in deep water (e.g., Craig et al., 1973) and sediment mixing and deposition rates (e.g., Miralles et al., 2005) and more recently ^{210}Po disequilibrium has been used to assess

* Corresponding author: Sylvain Rigaud Université de Nîmes - Laboratoire de Géochimie Isotopique Environnementale (GIS), 150 rue Georges Besse, 30035 NIMES Cedex 1, France. Tel.: +334 66 70 99 84; fax: +334 66 70 99 89.
E-mail address: sylvain.rigaud@unimes.fr (S. Rigaud).

http://dx.doi.org/10.1016/j.dsr2.2014.11.003
0967-0645/

particulate organic carbon (POC) export from the surface ocean (Shimmield et al., 1995; Friedrich and Rutgers van der Loeff, 2002; Stewart et al., 2007; Verdeny et al., 2009; Yang et al., 2011; Hu et al., 2014).

The activities of ^{210}Po and ^{210}Pb were first measured in the global ocean during the Geochemical Ocean Sections Study (GEOSECS) expeditions in the 1970s and have been widely measured since then in many marine systems. The most common features are ^{210}Pb excess with respect to ^{226}Ra in the surface ocean due to its atmospheric deposition and ^{210}Pb deficits at depth due to scavenging (Craig et al., 1973; Nozaki et al., 1976; Cochran et al., 1983; Cochran, 1992). In surface water, a deficit of ^{210}Po with respect to ^{210}Pb is commonly observed due to its preferential removal onto biogenic particles and lower atmospheric depositional flux of ^{210}Po compared to ^{210}Pb (e.g., Turekian and Nozaki, 1980; Chung and Finkel, 1988; Kim and Church, 2001; Stewart et al., 2010; Hong et al., 2013). In subsurface water, the degradation of these biogenic particles results in ^{210}Po regeneration to the dissolved phase that can be responsible for ^{210}Po excess with respect to ^{210}Pb (e.g., Bacon et al., 1976). In deep water, ^{210}Po was found to be in equilibrium with ^{210}Pb, although ^{210}Po deficiencies in deep waters have also been widely reported (Thomson and Turekian, 1976; Cochran et al. 1983; Chung and Finkel, 1988; Nozaki, et al., 1990; Kim, 2001; Chung and Wu, 2005; Hu et al., 2014). The causes for this deep ^{210}Po deficiency have been debated as due to methodological artifact, preferential scavenging of ^{210}Po in deep waters, and/or differential ^{210}Po and ^{210}Pb uptake by deep particles and adsorption at the sediment water interface. Such a deep ^{210}Po deficit was also reported during the recent GEOTRACES intercalibration cruises in both the North Pacific and North Atlantic involving many laboratories, suggesting that this is not linked to analysis artifact (Church et al., 2012). However, the process responsible for this deficit remains unclear, and for this disequilibrium to be observed, its time scale should be on the order of the mean-life of ^{210}Po (199 days). Generally, the disequilibrium between ^{210}Po and ^{210}Pb as well as between ^{210}Pb and ^{226}Ra in the ocean and at its interfaces are believed to be largely dependent on the origin and composition of particles and the local conditions (e.g., surface planktonic blooms, nepheloid layers, hydrothermal plumes). Those dependences need to be better understood in order to apply the nuclide pair as an accurate proxy to quantify biogeochemical processes involved in the cycles of trace elements and C in the ocean.

As such, the ^{210}Po and ^{210}Pb natural radionuclide pair was included as part of the GEOTRACES program. It included the analysis of ^{210}Po and ^{210}Pb in the dissolved (<0.45 μm) as well as two classes of particles size (0.8–51 μm and >51 μm) along with ancillary parameters including nutrients, dissolved oxygen, particulate organic carbon (POC), other particle-reactive radionuclides (e.g., ^{234}Th, ^{230}Th, ^{228}Th) and key trace elements (e.g., stable Pb). In addition, the sampling in the water column was conducted with high vertical resolution, especially with respect to benthic and hydrothermal interfaces. Sampling of aerosols along the cruise track for the analysis of ^{210}Pb and major and trace elements was also included. The high sampling density and diversity of parameters measured is expected to provide insight into several key biogeochemical processes and their time scales operating in the ocean including phase exchange rates.

This paper reports the dissolved, small and large particulate ^{210}Po and ^{210}Pb activities obtained along vertical profiles at the seven super stations (i.e., full depth stations with extra casts to provide large-volume samples) from the US GEOTRACES GA03 section in the North Atlantic Ocean. The main objectives of the present paper are to (1) improve the understanding of processes controlling the ^{210}Po and ^{210}Pb nuclide cycles in the North Atlantic Ocean and at its interfaces, (2) quantify the net rates of dissolved-particulate exchange and particle export and (3) compare the current distribution of these natural radionuclides in the North Atlantic Ocean to the distribution measured in the 1970s during GEOSECS.

2. Material and methods

2.1. Sampling

Sampling was performed during the US GEOTRACES GA03 North Atlantic section on the RV Knorr during October and November 2010 from Lisbon to Cape Verde (Leg1, KN199-4) and during November and December 2011 from Woods Hole, MA, to Cape Verde (Leg2, KN204-1).

Seawater samples for ^{210}Po and ^{210}Pb determination were collected at 7 super stations (Fig. 1; Table 1). They include three stations relatively close to the coast: (1) off Portugal, where Mediterranean Outflow Water (MOW) was observed between

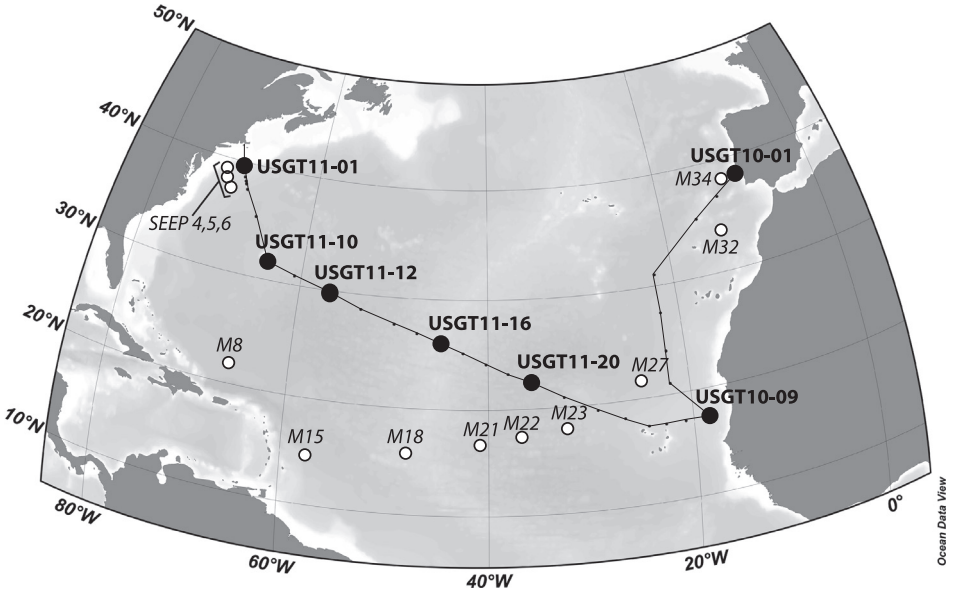

Fig. 1. The US GEOTRACES GA03 North Atlantic section with the location of the sampled super stations (dark dots). The location of METEOR (Bacon, 1977) and SEEP (Bacon et al., 1988) stations are also reported (white dots).

Please cite this article as: Rigaud, S., et al., ^{210}Po and ^{210}Pb distribution, dissolved-particulate exchange rates, and particulate export along the North Atlantic US GEOTRACES GA03 section. Deep-Sea Res. II (2015), http://dx.doi.org/10.1016/j.dsr2.2014.11.003

Table 1
Sampling information for the stations occupied during the US GEOTRACES GA03 transect. Mixed layer depth was calculated from surface potential density +0.125 (Hatta, pers. comm.).

Super station	Sampling date	Longitude (°W)	Latitude (°N)	Bottom depth (m)	Mixed layer depth (m)	Location
USGT11-01	07/11/11	69.7964	39.6924	2090	63	Off New England slope
USGT11-10	20/11/11	64.1902	31.7368	4530	80	Off Bermuda (BATS)
USGT11-12	24/11/11	56.8170	29.7000	5640	54.5	Mid-Western Basin
USGT11-16	29/11/11	44.8262	26.1368	3680	71.5	TAG
USGT11-20	04/12/11	35.8671	22.333	5450	69.5	Mid-Eastern Basin
USGT10-09	27/10/10	18.2542	17.3503	3050	30	Off Cape Verde
USGT10-01	17/10/10	9.6604	38.3299	2810	29.5	Off Portugal

500 and 1500 m depth (USGT10-01), (2) off Mauritania with anticipated Saharan dust inputs in surface, an oxygen minimum zone (OMZ; dissolved 0_2 concentrations $<100\,\mu M$) between 50 and 600 m depth and a benthic nepheloid layer (BNL) from 2900 m depth to bottom (USGT10-09) and (3) off New England on the continental slope (USGT11-01). Occupied as well were four open ocean stations in the oligotrophic western and eastern basins (USGT11-12 and USGT11-20, respectively), one close to Bermuda (USGT11-10, corresponding to the BATS/GEOTRACES base line station) and one at the Mid-Atlantic ridge where the Trans-Atlantic Geotraverse (TAG) hydrothermal plume was encountered between 3170 and 3440 m depth (USGT11-16).

At each station, sixteen 20 L seawater samples were collected throughout the water column using 30 L Niskin bottles mounted on a CTD rosette. In station USGT11-10, only the upper 2000 m water column was sampled for the dissolved phase. In stations USGT11-10 and USGT11–20, surface samples were also collected using a ship pump with a sampling tube that extended ~1–2 m below the surface. Once aboard, seawater was filtered using AcroPak 500 filter cartridges with a Supor 0.45 μm membrane attached to Teflon-lined Tygon tubing and acidified to pH2 using 6 N HCl within two hours after collection.

Small (0.8 to 51 μm) and large (>51 μm) particulate samples were simultaneously collected at approximately the same depths as the dissolved samples using MacLane in situ pumps. Particulate matter was collected on 142 mm diameter 0.8 μm pore size Supor (polyethersulfone) filters with a 51 μm mesh pre-screen, for small and large particles, respectively. Typical volumes filtered were ~500 L over a 4 h pumping period. Filters were processed at sea in a clean space, photographed and misted lightly to remove salts. One quarter of the filters were cut, dried at room temperature overnight in a laminar flow hood and then frozen at −20 °C for ^{210}Po and ^{210}Pb determination ashore.

2.2. Analysis

Samples for ^{210}Po and ^{210}Pb determination were processed at the University of Delaware for dissolved samples, at the Wayne State University for the small particulate samples and at the City University of New York for the large particulate fraction.

For dissolved samples, 10 L of filtered seawater were spiked with weighted aliquots of ^{209}Po (~1 dpm) and stable Pb (~10 mg) as yield monitors and allowed to equilibrate for >24 h. The Po and Pb isotopes were extracted from seawater by coprecipitation with $Fe(OH)_3$ as in the GEOTRACES inter-calibration exercise (Church et al., 2012). The precipitate was recovered by filtration (0.45 μm polycarbonate Nucleopore) and then dissolved in a 0.5 M HCl solution. In the case of particulate samples, analytical methods followed those described by Baskaran et al. (2013) for small particulate samples and Verdeny et al. (2008) for large particulate samples. Briefly, the samples were spiked with ^{209}Po and stable Pb before being dissolved using a mixture of strong acids (i.e., HF, HCl and HNO_3) on hot plates. Then, the residual filter material was discarded after being rinsed with concentrated acids and the solution was evaporated to near-dryness and recovered in 0.5 M HCl. The ^{210}Po and ^{209}Po are plated by spontaneous deposition from the 0.5 M HCl solution onto a silver disc (Flynn, 1968) and their activities were assayed by alpha spectroscopy. The remaining Po in solution is removed using AG-1 × 8 anion exchange resin as described in the intercalibration exercise by Church et al. (2012) for dissolved and small particulate samples or by introducing a piece of scrap silver into the solution for large particulate samples. Both of these methods yielded comparable results during the GEOTRACES intercalibration exercises. The final eluate solution is respiked with ^{209}Po and stored for at least 6 months to allow ingrowth of ^{210}Po from ^{210}Pb. Then ^{210}Pb activity of the samples is determined by plating the ^{210}Po produced in the eluate solution on another silver disc. Recovery of ^{210}Pb during sample processing was determined by measuring Pb concentrations in small aliquots of the plating solutions by atomic absorption spectroscopy (dissolved and small particulate) or inductively coupled plasma optical emission spectrometer (large particulate samples). Blank contamination was determined by processing several liters of pure water (dissolved samples) or dip blank filters (particulate samples) following the same procedure as for the field samples.

Finally, the initial activities and associated uncertainties of ^{210}Po and ^{210}Pb at the sampling time were calculated by correcting for detector backgrounds, nuclide decay, ingrowth and recoveries as well as for blank contamination (Rigaud et al., 2013; Baskaran, et al., 2013). Final ^{210}Po and ^{210}Pb activities are available as a supplementary web appendix. The data for ^{226}Ra and POC used in this paper was graciously provided by Charette et al. (in press) and Lam (n.d.), respectively. For the specific sampling and analytical methods, refer to those corresponding papers.

2.3. Mass balance calculations

Mass balance calculations were conducted to assess ^{210}Po and ^{210}Pb dissolved-small particulate and small-large particulate exchanges rates and large particle export rates, as well as the corresponding nuclides residence time in each phase. The approach used is similar to that previously published (Bacon and Anderson, 1982; Clegg and Whitfield, 1991; Cochran and Masque, 2003). The model conceptualization is represented in Fig. 2. It is assumed that:

(1) The system is in steady state with respect to the nuclide periods;
(2) Reversible ^{210}Po and ^{210}Pb exchange occurs between the dissolved and the small particulate phases by sorption vs desorption/regeneration processes;
(3) Reversible ^{210}Po and ^{210}Pb exchange takes place between small and large particulate phases by aggregation/disaggregation processes;

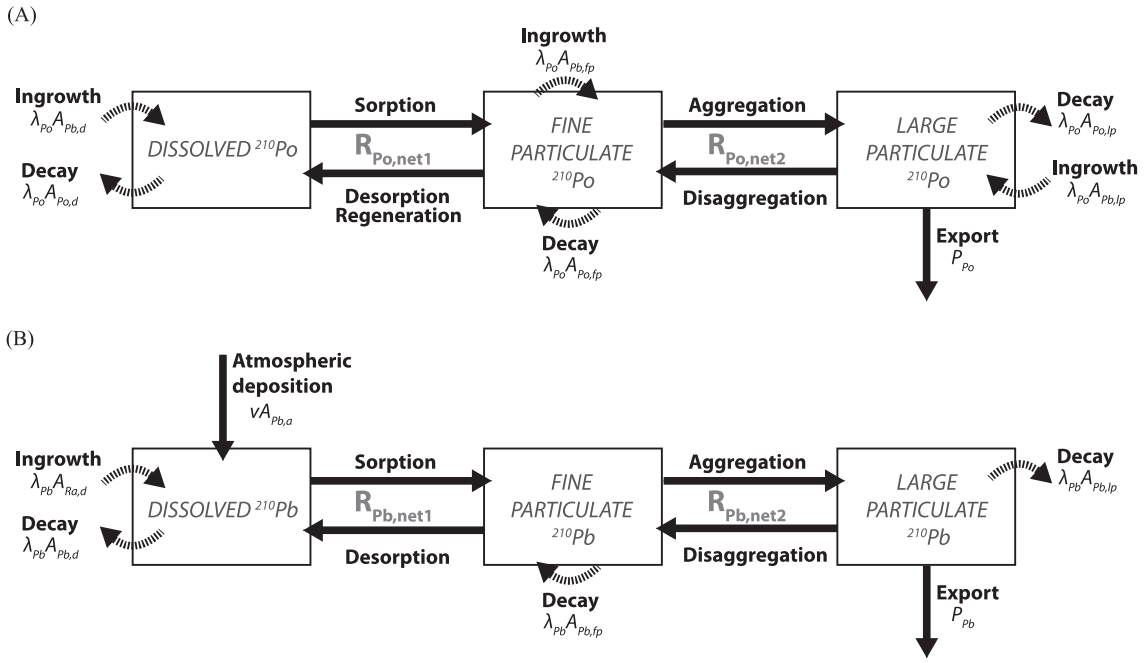

Fig. 2. Conceptualized model for the (A) ^{210}Po and (B) ^{210}Pb mass balance calculation into the dissolved, small and large particulate phases of the ocean water column. Terms and corresponding units are defined in Section 2.3.

(4) Only the large particles (>51 μm) sink while the small particles (from 0.8 to 51 μm) remain suspended in the water column;
(5) The horizontal and vertical advection and diffusive transports are minimal with respect to reactive and vertical particulate export processes;
(6) ^{226}Ra activity in the particulate phases is negligible (i.e., no ^{210}Pb ingrowth);
(7) ^{210}Pb atmospheric deposition only affects the upper water column and is assumed to be in the dissolved phase. The ^{210}Po atmospheric deposition is negligible since much of the time ^{210}Po/^{210}Pb in precipitation and aerosols is <0.1 (Baskaran, 2011).

Although the assumptions (1) and (5) may be assumed correct in open ocean stations, this is likely not the case in the upper water from the stations close to the coast. As we do not have spatial and temporal ^{210}Po and ^{210}Pb gradients or assessment of advection and diffusion coefficients at these stations, these assumptions cannot be evaluated at this time.

2.3.1. *Mass balance in the dissolved phase: Dissolved-small particulate exchange rates*

The mass balance equations for ^{210}Po and ^{210}Pb in the dissolved phase are given in Eqs. (1) and (2), respectively.

$$\left(\frac{\partial A_{\mathrm{Po},d}}{\partial t}\right)_z = \lambda_{\mathrm{Po}}A_{\mathrm{Pb},d} - \lambda_{\mathrm{Po}}A_{\mathrm{Po},d} - R_{\mathrm{Po},net1} \quad (1)$$

$$\left(\frac{\partial A_{\mathrm{Pb},d}}{\partial t}\right)_z = \lambda_{\mathrm{Pb}}A_{\mathrm{Ra},d} - \lambda_{\mathrm{Pb}}A_{\mathrm{Pb},d} - R_{\mathrm{Pb},net1} + \frac{I_{\mathrm{Pb}}}{z_S} \quad (2)$$

where $A_{\mathrm{Po},d}$, $A_{\mathrm{Pb},d}$ and $A_{\mathrm{Ra},d}$ are the ^{210}Po, ^{210}Pb and ^{226}Ra activities in the dissolved phase (dpm m^{-3}), λ_{Po} and λ_{Pb} are the decay constants of ^{210}Po and ^{210}Pb (1.83 y^{-1} and 3.11×10^{-2} y^{-1}, respectively), I_{Pb} is the ^{210}Pb atmospheric deposition (dpm m^{-2} y^{-1}) occurring over the surface mixed layer z_S (m) and $R_{\mathrm{Po},net1}$ and $R_{\mathrm{Pb},net1}$ are the net exchange rates at the dissolved-small particulate interface (dpm m^{-3} y^{-1}).

Assuming steady state conditions ($(\partial A_{\mathrm{Po},d}/\partial t)_z \cong 0$; $(\partial A_{\mathrm{Pb},d}/\partial t)_z \cong 0$) Eqs. (1) and (2) can be rewritten as

$$R_{\mathrm{Po},net1} = \lambda_{\mathrm{Po}}A_{\mathrm{Pb},d} - \lambda_{\mathrm{Po}}A_{\mathrm{Po},d} \quad (3)$$

$$R_{\mathrm{Pb},net1} = \lambda_{\mathrm{Pb}}A_{\mathrm{Ra},d} - \lambda_{\mathrm{Pb}}A_{\mathrm{Pb},d} + \frac{I_{\mathrm{Pb}}}{z_{\mathrm{MLD}}} \quad (4)$$

Positive $R_{\mathrm{Po},net1}$ and $R_{\mathrm{Pb},net1}$ values indicate net ^{210}Po and ^{210}Pb transfer from the dissolved phase to the small particle phase (i.e., sorption process dominates), while negative values correspond to net transfer from small particles to dissolved phase (i.e., desorption/regeneration process dominates).

2.3.2. *Mass balance in the small particulate phase: Small-large particulate exchange rates*

The mass balance equations for ^{210}Po and ^{210}Pb in the small particulate phase are given in Eqs. (5) and (6), respectively.

$$\left(\frac{\partial A_{\mathrm{Po},fp}}{\partial t}\right)_z = \lambda_{\mathrm{Po}}A_{\mathrm{Pb},fp} - \lambda_{\mathrm{Po}}A_{\mathrm{Po},fp} + R_{\mathrm{Po},net1} - R_{\mathrm{Po},net2} \quad (5)$$

$$\left(\frac{\partial A_{\mathrm{Pb},fp}}{\partial t}\right)_z = -\lambda_{\mathrm{Pb}}A_{\mathrm{Pb},fp} + R_{\mathrm{Pb},net1} - R_{\mathrm{Pb},net2} \quad (6)$$

where $A_{\mathrm{Po},fp}$ and $A_{\mathrm{Pb},fp}$ are the ^{210}Po and ^{210}Pb activities in the small particulate phase (dpm m^{-3}) and $R_{\mathrm{Po},net2}$ and $R_{\mathrm{Pb},net2}$ are the net exchange rates at the small-large particles interface (dpm m^{-3} y^{-1}). Assuming steady state conditions Eqs. (5) and (6) can be rewritten as

$$R_{\mathrm{Po},net2} = \lambda_{\mathrm{Po}}A_{\mathrm{Pb},fp} - \lambda_{\mathrm{Po}}A_{\mathrm{Po},fp} + R_{\mathrm{Po},net1} \quad (7)$$

$$R_{\mathrm{Pb},net2} = -\lambda_{\mathrm{Pb}}A_{\mathrm{Pb},fp} + R_{\mathrm{Pb},net1} \quad (8)$$

Positive $R_{\mathrm{Po},net2}$ and $R_{\mathrm{Pb},net2}$ values indicate ^{210}Po and ^{210}Pb net transfer from the small to the large particle phase (i.e., aggregation process dominates), while negative values correspond to net transfer from large to small particles (i.e., disaggregation process dominates).

Please cite this article as: Rigaud, S., et al., ^{210}Po and ^{210}Pb distribution, dissolved-particulate exchange rates, and particulate export along the North Atlantic US GEOTRACES GA03 section. Deep-Sea Res. II (2015), http://dx.doi.org/10.1016/j.dsr2.2014.11.003

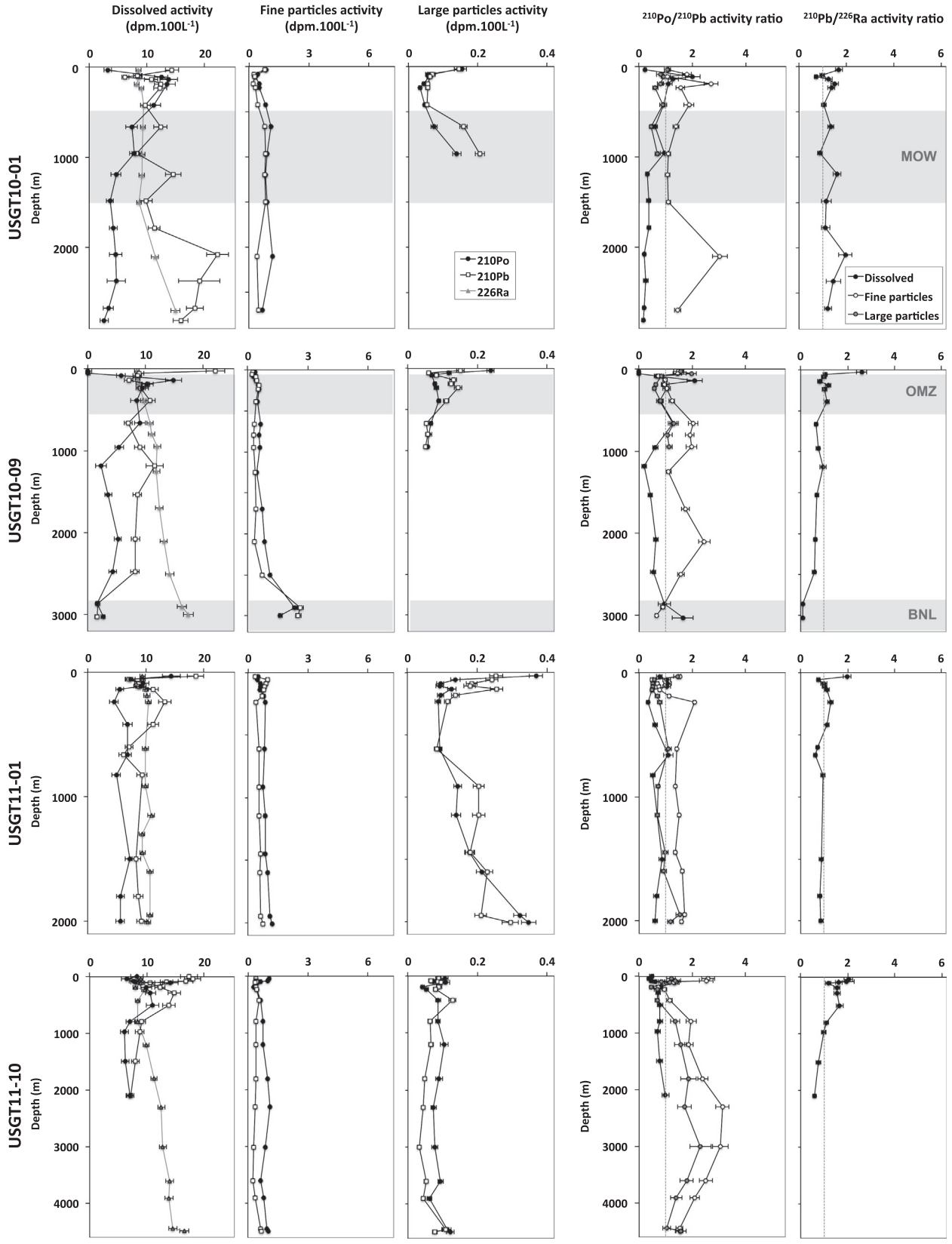

Fig. 3. ^{210}Po, ^{210}Pb and ^{226}Ra activities and corresponding ^{210}Po/^{210}Pb and ^{210}Pb/^{226}Ra activity ratio profiles in the dissolved, small and large particulate phases in the seven super stations occupied during the US GEOTRACES GA03 section. Specific areas are highlighted: MOW=Mediterranean outflow water; OMZ=oxygen minimum zone; BNL=benthic nepheloid layer; TAG=Trans-Atlantic Geotraverse hydrothermal plume. ^{226}Ra activities are from Charette (pers. comm.).

Please cite this article as: Rigaud, S., et al., ^{210}Po and ^{210}Pb distribution, dissolved-particulate exchange rates, and particulate export along the North Atlantic US GEOTRACES GA03 section. Deep-Sea Res. II (2015), http://dx.doi.org/10.1016/j.dsr2.2014.11.003

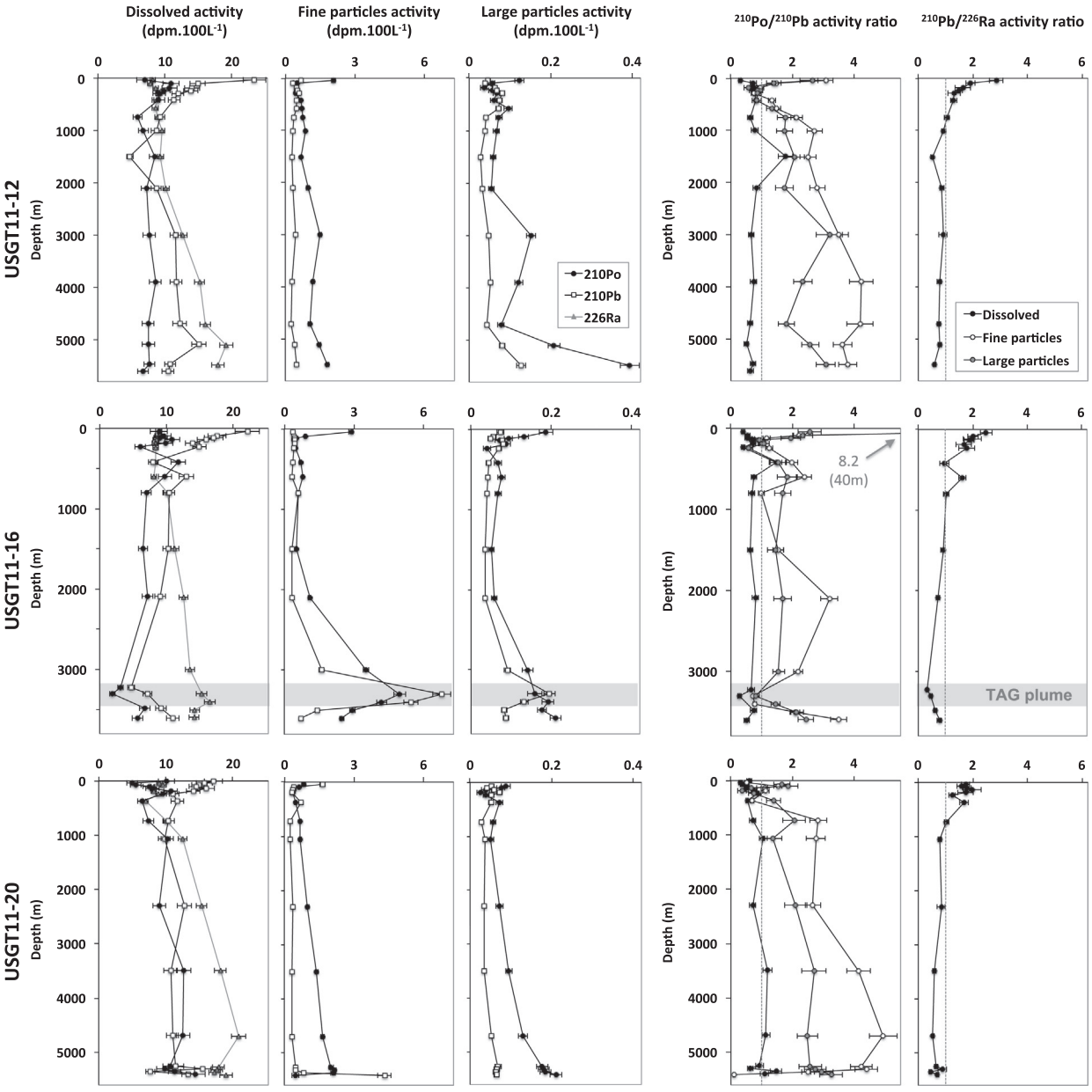

Fig. 3. (*continued*)

2.3.3. Mass balance in the large particulate phase: Large particulate export rates

The mass balance equations for ^{210}Po and ^{210}Pb in the large particulate phase are given in eqs. (9) and (10), respectively.

$$\left(\frac{\partial A_{\mathrm{Po},lp}}{\partial t}\right)_z = \lambda_{\mathrm{Po}} A_{\mathrm{Pb},lp} - \lambda_{\mathrm{Po}} A_{\mathrm{Po},lp} + R_{\mathrm{Po},net2} - P_{\mathrm{Po}} \tag{9}$$

$$\left(\frac{\partial A_{\mathrm{Pb},lp}}{\partial t}\right)_z = -\lambda_{\mathrm{Pb}} A_{\mathrm{Pb},lp} + R_{\mathrm{Pb},net2} - P_{\mathrm{Pb}} \tag{10}$$

where $A_{\mathrm{Po},lp}$ and $A_{\mathrm{Pb},lp}$ are the ^{210}Po and ^{210}Pb activities in the large particulate phase (dpm m^{-3}) and P_{Po} and P_{Pb} are the export of ^{210}Po and ^{210}^{210}Pb (dpm m^{-3} y^{-1}) with the large sinking particles. Assuming steady state conditions Eqs. (9) and (10) can be rewritten as

$$P_{\mathrm{Po}} = \lambda_{\mathrm{Po}} A_{\mathrm{Pb},lp} - \lambda_{\mathrm{Po}} A_{\mathrm{Po},lp} + R_{\mathrm{Po},net2} \tag{11}$$

$$P_{\mathrm{Pb}} = -\lambda_{\mathrm{Pb}} A_{\mathrm{Pb},lp} + R_{\mathrm{Pb},net2} \tag{12}$$

2.3.4. Residence time calculations

Corresponding residence times of nuclides in the dissolved ($\tau_{\mathrm{Po},d}$ and $\tau_{\mathrm{Pb},d}$), small ($\tau_{\mathrm{Po},fp}$ and $\tau_{\mathrm{Pb},fp}$) and large ($\tau_{\mathrm{Po},lp}$ and $\tau_{\mathrm{Pb},lp}$) particulate phases with respect to net exchange or export rates are obtained using Eqs. (13)–(15), respectively.

$$\tau_{\mathrm{Po},d} = \frac{A_{\mathrm{Po},d}}{R_{\mathrm{Po},net1}} \quad \text{and} \quad \tau_{\mathrm{Pb},d} = \frac{A_{\mathrm{Pb},d}}{R_{\mathrm{Pb},net1}} \tag{13}$$

$$\tau_{\mathrm{Po},fp} = \frac{A_{\mathrm{Po},fp}}{R_{\mathrm{Po},net2}} \quad \text{and} \quad \tau_{\mathrm{Pb},fp} = \frac{A_{\mathrm{Pb},fp}}{R_{\mathrm{Pb},net2}} \tag{14}$$

$$\tau_{\mathrm{Po},lp} = \frac{A_{\mathrm{Po},lp}}{P_{\mathrm{Po}}} \quad \text{and} \quad \tau_{\mathrm{Pb},lp} = \frac{A_{\mathrm{Pb},lp}}{P_{\mathrm{Pb}}} \tag{15}$$

Please cite this article as: Rigaud, S., et al., ^{210}Po and ^{210}Pb distribution, dissolved-particulate exchange rates, and particulate export along the North Atlantic US GEOTRACES GA03 section. Deep-Sea Res. II (2015), http://dx.doi.org/10.1016/j.dsr2.2014.11.003

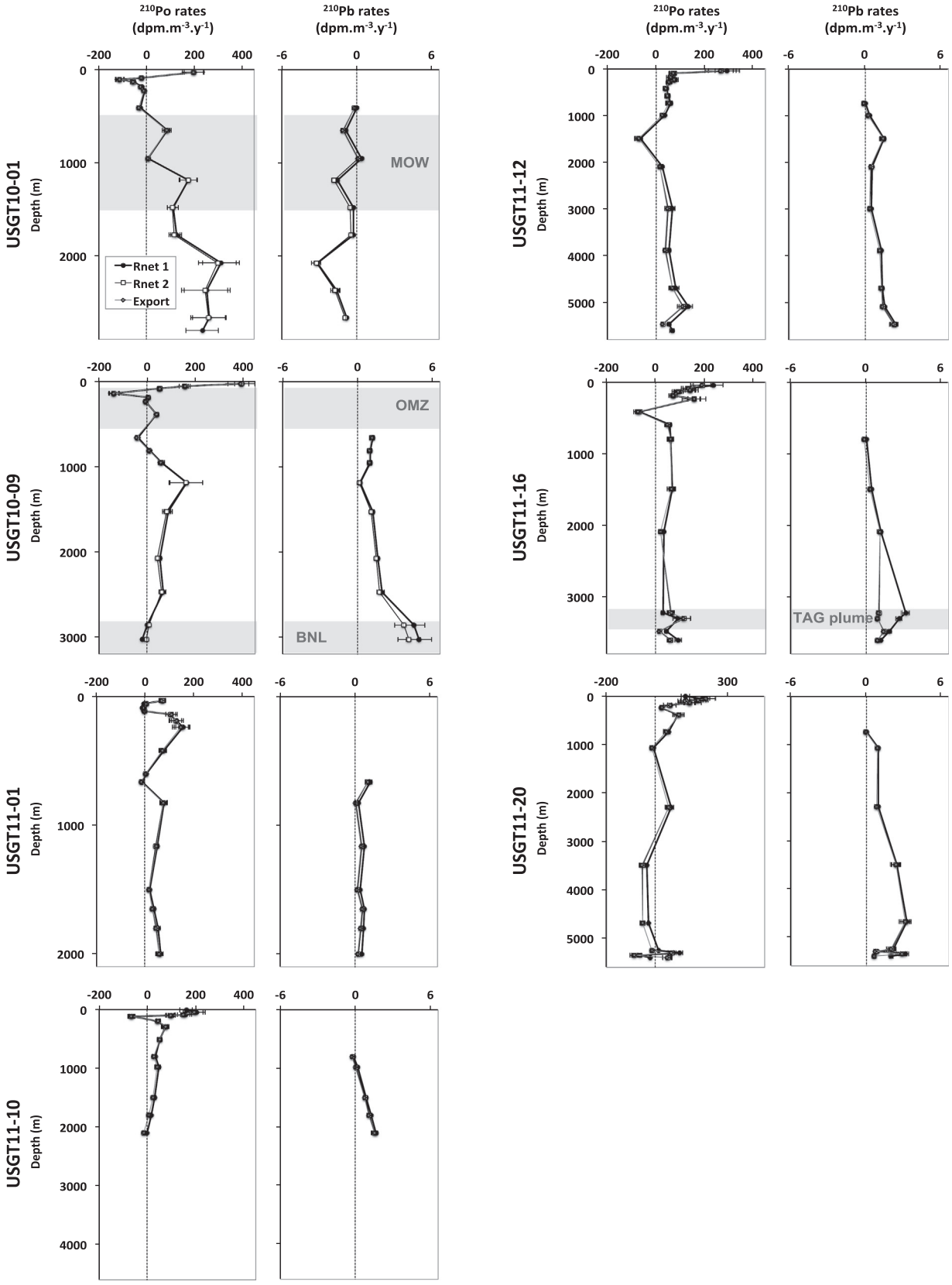

Fig. 4. Calculated ^{210}Po and ^{210}Pb net exchanges rates at the dissolved-small particulate interface (R_{net1}), the small-large particulate interface (R_{net2}) and export rates by large particle settling in the seven super stations occupied during the US GEOTRACES GA03 transect. Specific areas are also highlighted (cf. Fig. 3 legend).

Please cite this article as: Rigaud, S., et al., ^{210}Po and ^{210}Pb distribution, dissolved-particulate exchange rates, and particulate export along the North Atlantic US GEOTRACES GA03 section. Deep-Sea Res. II (2015), http://dx.doi.org/10.1016/j.dsr2.2014.11.003

3. Results

We first describe the ^{210}Po and ^{210}Pb distribution in the study area in general and then focus on specific observations for areas such as the MOW, the TAG plume and the BNL.

The vertical profiles of ^{210}Po, ^{210}Pb and ^{226}Ra activities as well as corresponding ^{210}Po/^{210}Pb and ^{210}Pb/^{226}Ra activity ratios at the 7 super stations are presented in Fig. 3. Typical ranges of ^{210}Po activities are ~0–14.9 dpm 100 L^{-1} in the dissolved phase, 0.3–5.0 dpm 100 L^{-1} in the small particulate phase, and 0.03–0.39 dpm 100 L^{-1} in the large particulate phase. For ^{210}Pb, these ranges are 1.6–23.4 dpm 100 L^{-1} in the dissolved phase, 0.2–6.8 dpm 100 L^{-1} in the small particulate phase, and 0.03–0.29 dpm 100 L^{-1} in the large particulate phase. The overall distribution between dissolved and particulate phases indicates that both nuclides are mainly present in the dissolved form, corresponding to 85 ± 16% and 93 ± 10% of their total activity in the water column for ^{210}Po and ^{210}Pb, respectively. Particulate ^{210}Po and ^{210}Pb activities correspond respectively to only 14 ± 13% and 7 ± 10% in the small particulate phase and 2 ± 5% and 0.8 ± 0.6% in the large particulate phase of the total activity. These general distributions mask locally distinct dissolved-particulate distributions such as some surface samples where the small particulate phase constitutes 15–70% of the total ^{210}Po activities and samples from the BNL (USGT10-09) and the TAG plume (USGT11-16) where small particles constitute 40–70% of the total ^{210}Po and ^{210}Pb activities.

The vertical profiles of dissolved ^{210}Po activities generally display the lowest activities in surface waters (< 100 m depth), the highest activities in subsurface layers (between 100 and 200 m depths) and near constant or decreasing activities at depth (Fig. 3). Profiles in the small and large particulate phases show an inverse trend with relatively high ^{210}Po activity in the surface, lowest activity in the subsurface and increasing activity with depth with highest values near the bottom. The vertical profiles of dissolved ^{210}Pb activity are characterized by the highest activities in the surface layer (< 100 m) and rather constant (between 8 and 12 dpm 100 L^{-1}) activities in the water column below (Fig. 3). Particulate ^{210}Pb profiles are similar to the ^{210}Po particulate profiles, but with most often significantly lower activities.

Corresponding ^{210}Po/^{210}Pb dissolved activity ratios are < 1 in the surface, ≥ 1 in the subsurface and mostly significantly < 1 at depth, with inverse trends in the particulate phases (Fig. 3). The ^{210}Po/^{210}Pb activity ratios in the small and large particulate phases follow the same trends with depth, although the range of the activity ratios is higher in the small particulate phase (from 0.1 to 8.2) than in the large particulate phase (from 0.5 to 3.3). The ^{210}Pb/^{226}Ra activity ratios in the dissolved phase generally show similar trends between stations with values > 1 in surface decreasing with depth generally becoming < 1 deeper than 500–1000 m depths (Fig. 3).

The range of activities, the general dissolved-particulate distribution, and the general vertical trend of ^{210}Po and ^{210}Pb are in good agreement with those previously reported in the North Atlantic (Bacon et al., 1976; Bacon et al., 1978; Hong et al., 2013; Kim, 2001) and other world oceans (e.g., Chung and Finkel, 1988; Cochran et al., 1983). However, several observations on the distribution of ^{210}Po and ^{210}Pb differ locally from the general patterns previously described:

The depth layers at the stations closest to the coast USGT10-01 within the MOW (between 500 and 1000 m depth), USGT10-09 within the OMZ (between 100 and 500 m depth) and USGT11-01 (between 800 and 1300 m depths), exhibit the largest enrichment of ^{210}Pb activities with respect to ^{210}Po in large particles (^{210}Po/^{210}Pb activity ratio < 1) (Fig. 3).

Below 500 m in station USGT10-01, the dissolved ^{210}Pb/^{226}Ra activity ratios are ≥ 1 in the water column in the MOW, increasing up to 2 below 2000 m depth, while the ratios are always ≤ 1 in the other stations for such depths.

The BNL between 2800 and 3100 m depth in station USGT10-09 shows extremely low (< 2.5 dpm 100 L^{-1}) dissolved ^{210}Po and ^{210}Pb activities and very high (> 1.6 dpm 100 L^{-1}) small particulate activities (data in the large particulate phase is not available at these depths). At these depths, the corresponding ^{210}Po/^{210}Pb activity ratios are ≥ 1 in the dissolved phase and ≤ 1 in the small particulate phase, while the ^{210}Pb/^{226}Ra activity ratios in the dissolved phase attain their lowest values (0.09).

The TAG hydrothermal plume between 3200 and 3500 m depth evidences very low ^{210}Po and ^{210}Pb dissolved activities corresponding to a large enrichment of both nuclides in the small and of ^{210}Pb in the large particulate phases. In the plume, one can observe a clear decrease of the ^{210}Po/^{210}Pb activity ratios in the dissolved, small and large particulate phases as well as a decrease of ^{210}Pb/^{226}Ra activity ratios in the dissolved phase, compared to water outside the plume.

The near bottom depth in station USGT11-20 displays a large increase of ^{210}Pb activities and large decrease of the ^{210}Po activities

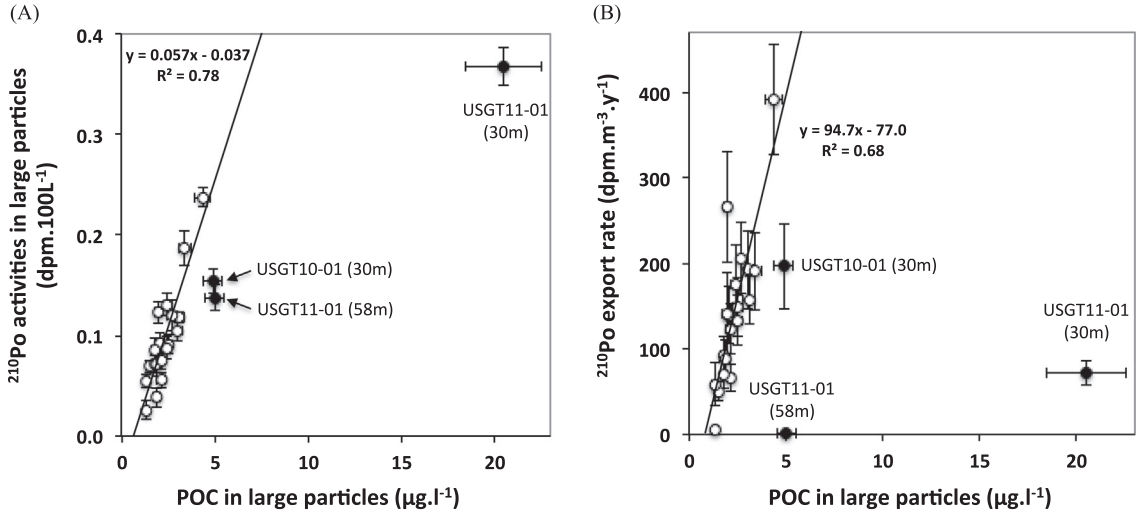

Fig. 5. Correlation between (A) ^{210}Po activities in large particles and (B) ^{210}Po export rates with the POC contents in the large particles from surface samples (i.e., located above the ^{210}Po regeneration peak). The three samples represented by black symbols are excluded from the correlation. They correspond to the samples from the stations close to the coast USGT11-01 (30 and 58 m depths) and USGT10-01 (30 m depth). The POC data are from Lam (n.d.).

Please cite this article as: Rigaud, S., et al., ^{210}Po and ^{210}Pb distribution, dissolved-particulate exchange rates, and particulate export along the North Atlantic US GEOTRACES GA03 section. Deep-Sea Res. II (2015), http://dx.doi.org/10.1016/j.dsr2.2014.11.003

in the small particulate phase corresponding to an intense decrease in the ^{210}Po/^{210}Pb activity ratio reaching very low values (0.11) near the bottom.

4. Discussion

The general processes and associated rates controlling the distribution of ^{210}Po and ^{210}Pb in surface, subsurface, and deep water in the whole section will be discussed first, while those specific to the MOW, the hydrothermal TAG plume and the BNL will follow.

The calculated net transfer rates at the dissolved-small particulate interface (R_{net1}, adsorption/desorption-regeneration processes), at the small-large particulate interface (R_{net2}, aggregation/disaggregation processes) and the large particles export rates for ^{210}Po and for ^{210}Pb are presented in Fig. 4. The primary observation is that for all stations and for both ^{210}Po and ^{210}Pb, the calculated R_{net1}, R_{net2} and export rates are generally similar within the uncertainties. This is mainly due to both nuclides being primarily present in the dissolved phase. Here the mass balance of ^{210}Po and ^{210}Pb in the dissolved phase controls the calculated rates at the dissolved-small particle interface, the small-large particle interface, as well as the export rates with large particle settling. Some differences however appear locally when the particulate activity becomes significant (e.g., BNL or TAG plume). In the following, these rates are referred to "scavenging" rates for subsequent sorption, aggregation and export rates (positive values) and as "regeneration" rates for subsequent desorption/release and disaggregation rates (negative values).

4.1. ^{210}Po cycling in surface and subsurface ocean

The widespread dissolved ^{210}Po deficit relative to ^{210}Pb in the surface waters, the increase of ^{210}Po activity in subsurface where ^{210}Po excess may appear, with inverse trends in the particulate phase, are similar to those previously reported in the North Atlantic (Bacon et al., 1976; Kim, 2001; Kim and Church, 2001; Stewart et al., 2010; Hong et al., 2013) and in other oceans (Turekian and Nozaki, 1980; Cochran et al., 1983; Chung and Finkel, 1988; Murray et al., 2005). They have been attributed to the preferential transfer of ^{210}Po from the dissolved to the particulate phase by biological uptake in surface waters and export to subsurface waters by settling particles (i.e., scavenging). In subsurface water, the remineralization of particulate matter results in a release of ^{210}Po from the particles to the dissolved phase (Bacon et al., 1976, 1978, 1988; Cochran et al., 1983; Stewart and Fisher, 2003a; Stewart et al., 2005).

The ^{210}Po net scavenging rates calculated at the surface indicate a large variation in their intensity between all 7 stations (Fig. 4). However, in all stations the highest rates are always found in the uppermost samples and then decrease with depth, which supports the role of biological activity in ^{210}Po scavenging. The comparison between ^{210}Po scavenging rates and ^{210}Po activities in the large particles with the corresponding POC content (assumed to be the most important carrier for ^{210}Po scavenging) in surface samples indicates significant positive linear relationships (Fig. 5A and B, except the for the two stations closest to the coast discussed as a specific case later). The POC collected in the surface water is normally a heterogeneous mixture of phytoplankton species, non-photosynthetic living species (e.g., bacteria, zooplankton) and detrital organic particles that can all contain actively bioaccumulated ^{210}Po. The fact that a positive linear relationships exists suggests that the large particle POC composition is likely relatively homogeneous over stations and with a similar capacity for ^{210}Po scavenging. Note that no positive linear relationship exists between POC concentrations and ^{210}Pb activities in large particles ($r^2 < 0.15$; not shown). This further supports the role of bioaccumulation processes in the removal of ^{210}Po from the surface water of the North Atlantic, in addition to just physicochemical sorption.

In contrast, three surface samples from the stations closest to the coasts (30 m and 58 m depths in USGT11-01 and 30 m depth in USGT10-01) do not follow such linear correlations (Fig. 5A and B). These samples contain relatively high POC content with relatively low ^{210}Po scavenging rates and low ^{210}Po activities in large particles compared to the other samples. Several hypotheses may be involved to explain such discrepancies. Firstly, these stations may be characterized by POC with a different biological composition (planktonic species) or origin (e.g., terrestrial) that may be less efficient in the uptake of ^{210}Po in comparison to more open ocean stations. A second explanation could be associated to vertical mixing between surface and subsurface water leading to a decrease in the ^{210}Po surface deficit (Kadko, 1993a) and thus to a lower calculated ^{210}Po scavenging rates. Also, the input of ^{210}Po depleted particles from subsurface to surface, would lead to a relative decrease of the ^{210}Po particulate activities in surface samples. Such vertical mixing is more likely to occur in coastal environment. A third explanation could be associated to temporal changes in the physical and biogeochemical conditions in these stations over the months preceding the sampling that are effectively integrated by the relatively long-lived ^{210}Po (i.e., memory effect of the ^{210}Po signal over months). This indicates that despite the mechanistic relationship between ^{210}Po and C (both bioaccumulated) which may justify the use of ^{210}Po as a POC tracer (e.g., Kim, 2001; Friedrich and Rutgers van der Loeff, 2002, Verdeny

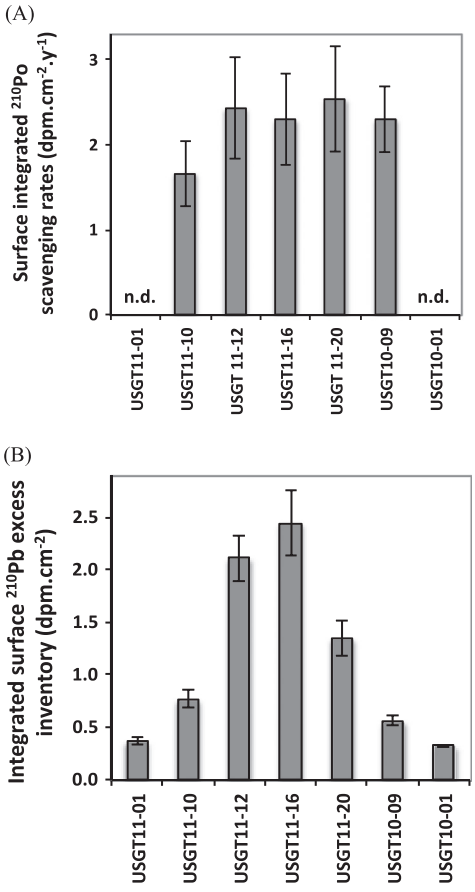

Fig. 6. Surface integrated (A) ^{210}Po scavenging rates and (B) ^{210}Pb excess inventory. The surface layers considered for the integration correspond to the layers where ^{210}Po scavenging occur (i.e., above the ^{210}Po regeneration peak) for (A) and to the surface layer where ^{210}Pb excess occurs for (B).

Please cite this article as: Rigaud, S., et al., ^{210}Po and ^{210}Pb distribution, dissolved-particulate exchange rates, and particulate export along the North Atlantic US GEOTRACES GA03 section. Deep-Sea Res. II (2015), http://dx.doi.org/10.1016/j.dsr2.2014.11.003

Table 2
Integrated net ^{210}Po sorption (R_{net1}), aggregation (R_{net2}) and large particles export with corresponding residence time in the dissolved, small and large particulate phases obtained for the surface layers at super stations along the North Atlantic US GEOTRACES GA03 section. The rates and residence times are based on the nuclide inventories integrated over the depth interval listed in column #2.

	Surface layer (m)	Dissolved		Small particles		Large particles	
		R_{net1} (dpm cm^{-2} y^{-1})	T_{res} (y)	R_{net2} (dpm cm^{-2} y^{-1})	T_{res} (d)	Export (dpm cm^{-2} y^{-1})	T_{res} (d)
USGT11-01	0–60	0.33 ± 0.04	1.9 ± 03	0.32 ± 0.05	27 ± 5	0.33 ± 0.06	18 ± 4
USGT11-10	0–100	1.8 ± 0.3	0.39 ± 0.08	1.7 ± 0.3	22 ± 4	1.7 ± 0.4	2.1 ± 0.5
USGT11-12	0–150	2.6 ± 0.4	0.5 ± 0.1	2.4 ± 0.5	28 ± 5	2.4 ± 0.6	1.9 ± 0.5
USGT11-16	0–150	2.6 ± 0.4	0.53 ± 0.10	2.3 ± 0.4	39 ± 7	2.3 ± 0.5	3.3 ± 0.9
USGT11-20	0–150	2.5 ± 0.4	0.37 ± 0.08	2.5 ± 0.5	15 ± 3	2.5 ± 0.6	1.9 ± 0.5
USGT10-09	0–100	2.3 ± 0.2	0.07 ± 0.03	2.3 ± 0.3	5.6 ± 0.9	2.3 ± 0.4	2.5 ± 0.4
USGT10-01	0–100	1.2 ± 0.2	0.47 ± 0.10	1.1 ± 0.3	22 ± 5	1.1 ± 0.3	3.7 ± 1.0
Average ± 1 sd		**1.9 ± 0.9**	**0.6 ± 0.6**	**1.8 ± 0.8**	**23 ± 10**	**1.8 ± 0.8**	**5 ± 6**

et al., 2009), the specific POC origin and composition, the occurrence of vertical mixing and the relatively long half-life of ^{210}Po may limit the suitable use of this tracer in highly dynamic systems.

Focusing on the subsurface water (generally between 100 and 200 m depth), the ^{210}Po scavenging rates strongly decrease in all stations compared to the surface layer. The negatives rates from −140 to −5 dpm m^{-3} y^{-1} at stations close to the coast and near Bermuda, indicate net ^{210}Po regeneration rates (Fig. 4). For the other stations, the net rates of ^{210}Po in the subsurface remains positive indicating that, although ^{210}Po regeneration occurs, the scavenging process dominates. As found here, subsurface ^{210}Po excess and net regeneration rates have been previously reported in literature (Thomson and Turekian, 1976; Bacon et al., 1976, 1980, 1988; Cochran et al., 1983; Chung and Finkel, 1988; Murray et al., 2005). For the North Atlantic, ^{210}Po subsurface excess was often noted in most of the North Atlantic stations studied by Bacon et al. (1976) but was not observed at BATS (Kim and Church, 2001; Stewart et al., 2010; Hong et al., 2013). Such ^{210}Po excess generally occur in subsurface waters when the water column is well stratified and intense particulate remineralization occurs (Cochran et al., 1983; Kadko, 1993a). Such a situation was encountered at station USGT10-09 that also presented the highest ^{210}Po subsurface regeneration rates in subsurface near the upper boundary of the OMZ (Fig. 4), supporting the link between subsurface ^{210}Po regeneration and organic material degradation. This ^{210}Po regeneration may be responsible for the significant ^{210}Po deficit observed in the large particles within the OMZ, and in subsurface waters at the two others coastal stations, USGT10-01 and USGT11-01 (Fig. 3).

In order to assess the ^{210}Po export from the surface at the four open ocean stations and the station off Mauritania (USGT10-09), we integrated the ^{210}Po scavenging rates over the surface layer where scavenging occurs (i.e., above the subsurface regeneration peak). In these five stations, the ^{210}Po scavenging rates range from 1.7 to 2.6 dpm cm^{-2} y^{-1} (Table 2, Fig. 6A). These estimates are in good agreement with those previously reported for the North Atlantic (1.2 dpm cm^{-2} y^{-1}, Bacon et al., 1976) and at BATS station (2.0–3.2 dpm cm^{-2} y^{-1} by Stewart et al., 2010 and 1.8–3.1 dpm cm^{-2} y^{-1} by Kim and Church, 2001). Corresponding residence times of ^{210}Po range from 0.07 to 0.53 y in the dissolved phase, from 6 to 39 d in the small particulate phase and from 2.0 to 3.3 d in the large particulate phase.

4.2. ^{210}Pb cycling in the surface ocean

As previously reported, in all stations excess ^{210}Pb over ^{226}Ra is observed in surface water. These excesses differ slightly between stations (Fig. 3) but vary strongly with depth in the water column. For example, ^{210}Pb excesses are only observed in the uppermost sample in stations closest to the coast USGT10-01, USGT10-09 and USGT11-01 (≤ 30 m depth) but can be maintained down to 400–500 m depth in the open ocean stations. Comparison between dissolved ^{210}Pb excess (^{210}Pb/^{226}Ra activity ratio in the dissolved phase) and dissolved Al concentrations (Measures et al., n.d.) in the mixed surface water shows a relatively good positive correlation (r^2=0.71, plot not shown). As Al is mainly provided to the surface ocean by atmospheric deposition, this indicates that ^{210}Pb distribution in the surface mixed layer is likewise controlled. Turekian et al. (1977) predicted the ^{210}Pb atmospheric deposition in North Atlantic to be between ~1 dpm cm^{-2} y^{-1} in the western Atlantic shore decreasing to about ~0.5 dpm cm^{-2} y^{-1} in the eastern Atlantic. These deposition rates are based on the estimated ^{222}Rn emanation rates from the continents, atmospheric circulation rates and aerosol mean residence times in the mid-northern hemisphere. This trend is generally supported by measurements (Benninger, 1978; Turekian et al., 1983; Hartman, 1987; Todd et al., 1989; Preiss and Genthon, 1997; Kim et al., 1999; Renfro et al., 2013; Lozano et al., 2013) and the general distribution of ^{210}Pb activity in aerosol in the Northern hemisphere (Baskaran, 2011). Note that seasonally higher depositions are also expected close to the eastern coast due to aerosol inputs from African (i.e., Saharan dust) and European air masses (Lozano et al., 2013).

Our observation of the geographic distribution of ^{210}Pb excess inventory in surface waters where the excess occurs does not follow the expected pattern from this theoretical model. Indeed, the integrated ^{210}Pb excess inventories in the dissolved phase are higher in the open ocean stations in comparison to those closer to the coast (Fig. 6B). The corresponding integrated excess ^{210}Pb supply rates (expressed by $\lambda_{210Pb}(A_{Pb}-A_{Ra})$, where λ_{210Pb} is the decay constant of ^{210}Pb and A_{Pb} and A_{Ra} are the integrated activity of dissolved ^{210}Pb and ^{226}Ra in the surface water) are at least two orders of magnitude lower than the expected atmospheric deposition (integrated excess rates of 0.01–0.08 dpm cm^{-2} y^{-1} compared to an atmospheric deposition of 0.5–1.0 dpm cm^{-2} y^{-1}). Assuming a constant ^{210}Pb atmospheric deposition rate of 0.5 dpm cm^{-2} y^{-1} in the North Atlantic, this indicates that >90% of the ^{210}Pb originating from atmospheric deposition is scavenged in the surface ocean. Corresponding dissolved ^{210}Pb residence times in the surface mixed layer are 1–2 y in stations close to the coast, and 3–6 y in open ocean stations, which is close to the averaged 2.5 years reported by Bacon et al. (1976). These results suggest that almost all the ^{210}Pb deposited from the atmosphere is rapidly scavenged within a few years in the upper ocean and that these scavenging rates are higher at ocean margins due to higher particle concentrations, in agreement with previous findings (Bruland et al., 1974; Bacon et al., 1976; Nozaki et al., 1976; Spencer, et al., 1981; Cochran et al., 1990; Henderson and Maier-Reimer, 2002).

Please cite this article as: Rigaud, S., et al., ^{210}Po and ^{210}Pb distribution, dissolved-particulate exchange rates, and particulate export along the North Atlantic US GEOTRACES GA03 section. Deep-Sea Res. II (2015), http://dx.doi.org/10.1016/j.dsr2.2014.11.003

4.3. ^{210}Po in deep water

In most of the samples from the deep water (> 500 m depth), ^{210}Po exhibits a significant deficit with respect to ^{210}Pb in the dissolved phase (Fig. 3). These ^{210}Po deficits are particularly evident from the ^{210}Po/^{210}Pb activity ratios integrated over the deep (> 500 m depth) water column (Fig. 7). When considering the total inventory (dissolved + fine and large particles), the ^{210}Po deficit remains significant. Only one station, USGT11-20, presents ^{210}Po activity without significant deficit in the dissolved and total phases. Excluding this station, the corresponding ^{210}Po mean residence times are 1.2 y in the dissolved phase, 80 d in the small particulate phase and 8 d in the large particulate phase.

These results differ from the total ^{210}Po equilibrium with respect to ^{210}Pb that was previously reported in the deep North Atlantic (Bacon et al., 1976; 1978; 1988), central and eastern Indian Ocean (Cochran et al., 1983), and eastern South Pacific (Turekian and Nozaki, 1980). They are however in agreement with observations from the benthic layers in the Western Indian Ocean (Chung and Finkel, 1988), from the deep water in the Sargasso sea (Kim, 2001), the South China Sea (Chung and Wu, 2005), the Aleutian basin (Hu et al., 2014), and from the GEOTRACES intercalibration deep samples at the SAFe and BATS stations (Church et al., 2012).

Kim (2001) hypothesized that the deficiency observed in the mesopelagic water layer (down to 2000 m depth) in oligotrophic environments is mainly due to ^{210}Po transfer from bacteria or cyanobacteria to higher trophic levels of organisms in the food web. In eutrophic environments, such deficit is observed to be lower or absent because ^{210}Po, as an element of the sulfur group, may reside in the free-living, non settling bacteria for longer periods (Kim, 2001). However, this specific hypothesis cannot be supported here as ^{210}Po deficits are observed at depth both in eutrophic stations close to the coast and in oligotrophic open ocean stations, in samples as deep as 5600 m depths, and because ^{210}Po equilibrium was also found in the oligotrophic station USGT11-20.

Both Chung and Finkel (1988) and Hu et al., (2014) suggest that the ^{210}Po deficiency in deep layers was attributed to preferential scavenging of ^{210}Po by sinking particles. The preferential ^{210}Po sorption onto particles, and then export, with respect to ^{210}Pb is supported here by the ^{210}Po excess relative to ^{210}Pb in both the small and large particulate phases, which is maintained throughout the water column (Fig. 3). In addition, the averaged large particle mass concentration over the deep water column indicates that it is the lowest at station USGT11-20 and the highest at station USGT10-01 (1.1 ± 0.2 and $11 \pm 5\ \mu g\ L^{-1}$, respectively, Lam, n.d.), supporting the fact that the concentration of large particulate matter (and thereby large particle flux) may in part be involved in the overall disequilibrium between ^{210}Po and ^{210}Pb in the deep water column. It is also worth noting that the ^{210}Po deficiency at depth is particularly evident at station USGT10-09, with high productivity at the surface and OMZ in the subsurface, similar to what was reported by Sarin et al. (1994) and Thomson and Turekian (1976). Although we still cannot fully explain the deficit of ^{210}Po in deep water there is evidence that both local particle scavenging and high surface productivity related phenomenon are involved. This is a major issue that GEOTRACES may be able to address in the future with a more detailed investigation into the chemical composition of the particles.

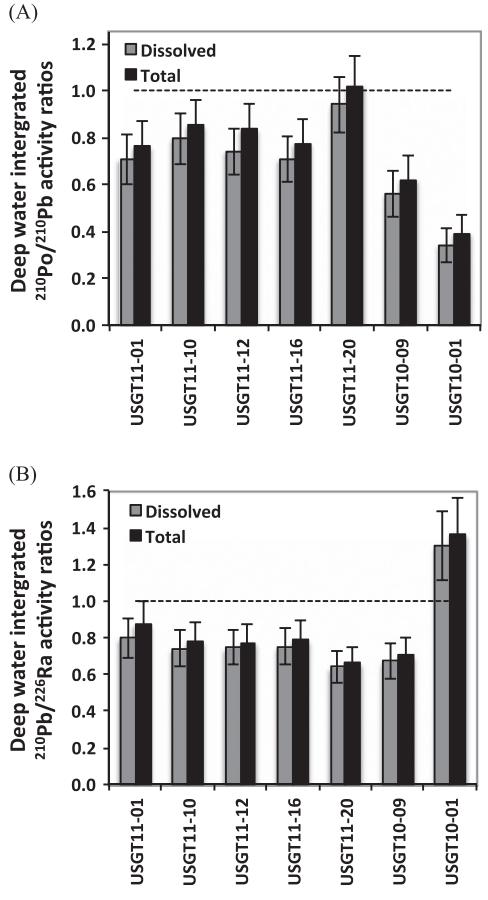

Fig. 7. (A) ^{210}Po/^{210}Pb and (B) ^{210}Pb/^{226}Ra activity ratios obtained from the dissolved and total inventories of nuclide activities over the deep water (> 500 m depths). Samples from the BNL (station USGT10-09) and the TAG plume (station USGT11-16) are excluded from the calculation. Note that for station USGT11-10, the water layer considered for the integration is between 500 and 2000 m depths (no dissolved data below 2000 m depth). In station USGT10-01 and USGT10-09, the total ^{210}Po do not account for large particulate phase below 1000 m that were not measured.

4.4. ^{210}Pb in deep water

Below the surface waters, the ^{210}Pb excess decreases to reach equilibrium with ^{226}Ra between 100 m and 1000 m depth depending on the station and then maintains a deficit down to the bottom (Fig. 3). According to the strong particle affinity of ^{210}Pb, the ^{210}Pb deficit in deep water is attributed to scavenging by adsorption with settling particles. Besides the station off Portugal (USGT10-01), two main patterns can be distinguished in the spatial distribution of the ^{210}Pb scavenging in deep water: (1) The calculated ^{210}Pb scavenging rates increase with depth to reach the highest value close to the bottom (Fig. 4), and (2) the integrated ^{210}Pb deficit relative to ^{226}Ra in deep water increases from the western to eastern North Atlantic (Fig. 7B).

The increase of the scavenging rates with depth has been attributed to enhanced ^{210}Pb scavenging associated with increased adsorptive particles in the benthic boundary layer and/or potentially with co-precipitation of ^{210}Pb with Fe and Mn oxides at the sediment-water interface (Bacon et al., 1976; Spencer et al., 1981; Cochran et al., 1983; Chung, 1987; Bacon et al., 1988). As both suspended matter and particulate Fe contents increased in the benthic layer (Lam, n.d; Ohnemus and Lam, n.d.), the enhanced ^{210}Pb scavenging at depth in all stations can be attributed to such an increase of available particulate surface area for ^{210}Pb adsorption. The increase of ^{210}Pb scavenging with the increase of suspended particle matter is further supported by the findings for the BNL and the TAG plume (see Sections 4.6 and 4.7).

The increase of ^{210}Pb deficit eastward in the North Atlantic deep water has not been reported before and suggests a relatively higher ^{210}Pb scavenging rates in the eastern basin than in to the western basin in the North Atlantic. This may be due to the higher

Please cite this article as: Rigaud, S., et al., ^{210}Po and ^{210}Pb distribution, dissolved-particulate exchange rates, and particulate export along the North Atlantic US GEOTRACES GA03 section. Deep-Sea Res. II (2015), http://dx.doi.org/10.1016/j.dsr2.2014.11.003

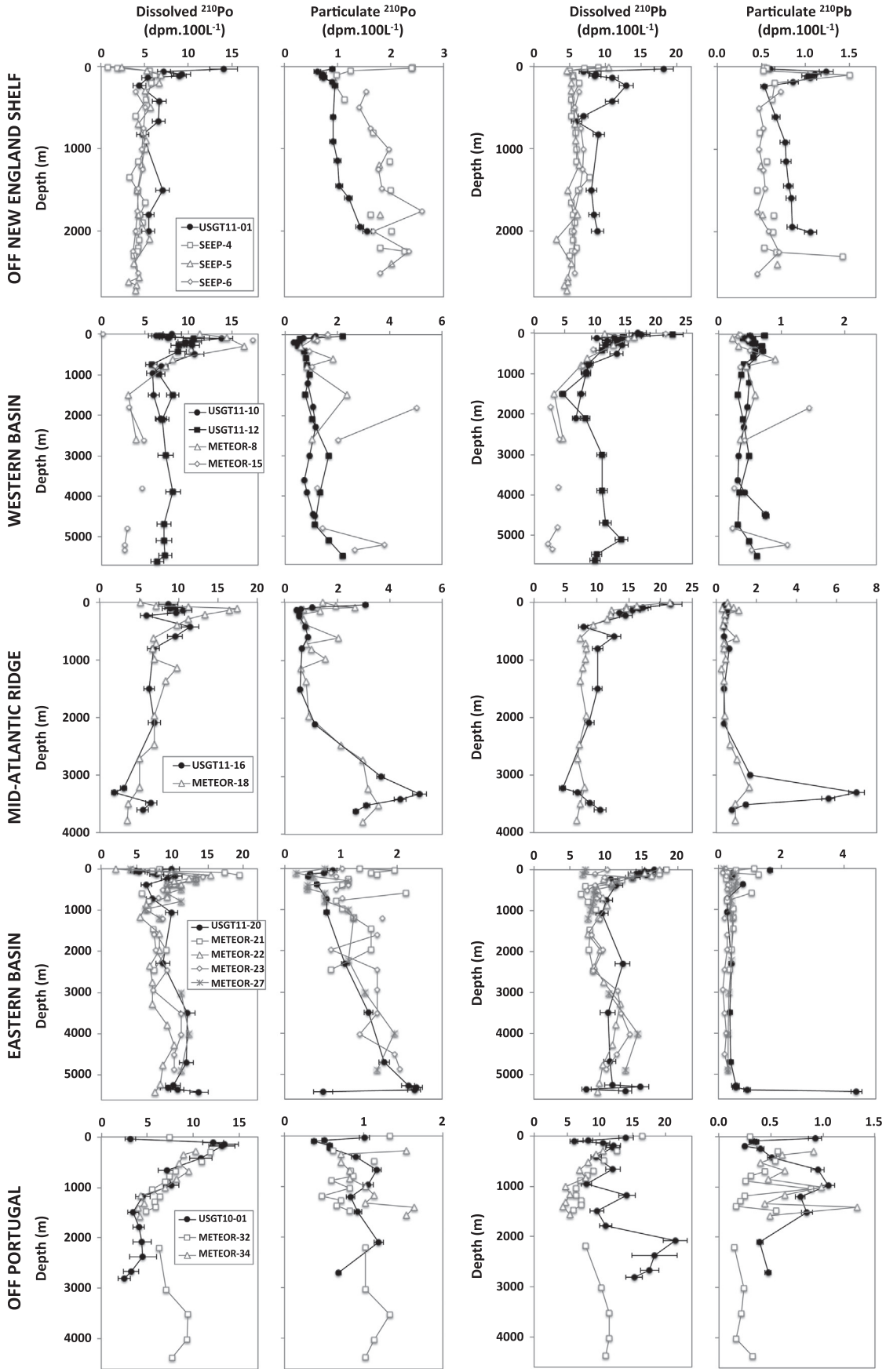

Fig. 8. Comparison of the dissolved and particulate ^{210}Po and ^{210}Pb activities obtained within the present study (USGT stations, in black) with those previously published by Bacon (1977) and Bacon et al. (1988) (METEOR and SEEP stations, respectively, in grey) in several sub-areas in the North Atlantic. The locations of the stations are reported in Fig. 1. USGT Particulate samples correspond to the sum of the small and large particulate fractions, excepted for the particulate samples deeper than 1000 m in station USGT10-01 for which large particulate data is not available.

Please cite this article as: Rigaud, S., et al., ^{210}Po and ^{210}Pb distribution, dissolved-particulate exchange rates, and particulate export along the North Atlantic US GEOTRACES GA03 section. Deep-Sea Res. II (2015), http://dx.doi.org/10.1016/j.dsr2.2014.11.003

lithogenic particle fluxes reported in the eastern basin related to higher aerosol inputs (Ohnemus and Lam, n.d.) and/or to higher benthic scavenging efficiency in the eastern basin.

These two patterns lead to a general decrease of the residence time of ^{210}Pb with depth and eastward. As a whole, from west to east, the residence time of ^{210}Pb in the deep water range from 130 to 60 y in the dissolved phase, from 13 to 2 y in the fine particulate phase and from 5 to 0.1 y in the large particulate phase. These values are in good agreement with the 15–100 y reported for the world deep ocean (Craig et al., 1973; Cochran, et al. 1990).

4.5. The Mediterranean outflow water (MOW)

Between 500 and 1800 m depth at station USGT10-01 the MOW was encountered, primarily indicated by higher salinity and temperature and lower O_2 concentrations (Jenkins et al., n.d.). It is also characterized by high dissolved trace element concentrations (e.g., Measures et al., n.d.; Hatta et al. n.d.; Noble et al., this issue) and high suspended matter content comprised mainly of inorganic material (Lam, n.d.). These particles likely originate from resuspended sediment on the continental margin of the Gulf of Cadiz or from the Mediterranean Sea itself (Thorpe, 1976; Schmidt, 2006). The MOW is also characterized by high particulate ^{210}Po and ^{210}Pb activities that are close to equilibrium in the small particulate phase but with a significant deficit of ^{210}Po relative to ^{210}Pb in the large particles in contrast to particles in waters adjacent to the MOW (Fig. 3). The secular equilibrium found in the small particles may be associated with older resuspended particles. However, the deficit in the large particulate phase is hard to explain and may reflect preferential ^{210}Po loss during degradation of the organic material (as observed within the OMZ in station USGT10-09) in the subsurface water in the Mediterranean (Stewart et al., 2007) and perhaps maintained during the transit of water (within months). Most striking in this water mass is the dissolved ^{210}Pb profile, exhibiting mostly equilibrium with respect to ^{226}Ra within the MOW and large unsupported activities below the MOW. This pattern is quite unique as ^{210}Pb is generally deficient in deep water, and is in contrast with the generally accepted view of considerable scavenging of ^{210}Pb at ocean margins with abundant sources of suspended material. Such observations also differ from those previously reported by Bacon (1977) in a neighboring station and by Gascó et al. (2002) in the MOW at the vicinity of the Gibraltar strait that generally showed lower ^{210}Pb dissolved activity within the MOW. This could suggest specific processes occurring on seasonal or annual timescales within and below the MOW that merit further investigation.

4.6. Benthic nepheloid layer (BNL)

From the CTD transmissometer data over the seven super stations where ^{210}Po and ^{210}Pb were measured, a BNL was found in station USGT10-09, starting from 2860 m depth to the bottom with the highest particle density encountered between 2990 and 3010 m depths. Two samples were collected within the BNL, one at ~2900 m and the second one at ~3000 m depth. In these samples, intense ^{210}Pb scavenging rates were calculated, with the highest rates corresponding to the deepest sample (Fig. 3). These processes are associated with the sorption of ^{210}Pb onto small particles that increased in mass from ~6 $\mu g\,L^{-1}$ in the overlying water to 10 $\mu g\,L^{-1}$ at 2900 m depth and 32.6 $\mu g\,L^{-1}$ at 3000 m depth (Lam, n.d.). The ^{210}Pb residence times are estimated at 3.2 ± 0.3 y in the dissolved phase and 6.5 ± 0.7 y in small particulate phase (absence of large ^{210}Po and ^{210}Pb particulate data here). This indicates that the BNL significantly enhances the ^{210}Pb scavenging in the deep eastern North Atlantic Ocean by a factor of 10–20. Such findings are in agreement with previous reports (Bacon et al., 1976; Spencer et al., 1981; Cochran et al., 1983; Chung, 1987; Bacon et al., 1988).

In contrast to ^{210}Pb, ^{210}Po does not show significant scavenging in the BNL (Fig. 4). In fact, ^{210}Po is found at equilibrium with ^{210}Pb in both the dissolved and particulate phases in the sample at 2900 m depth. In the sample at 3000 m depth, ^{210}Po is found in slight excess in the dissolved phase with a corresponding deficit in the particulate phase (Fig. 3). In the BNL, the total ^{210}Po is thus at equilibrium with ^{210}Pb (^{210}Po/^{210}Pb activity ratios = 0.99 ± 0.08). This indicates that the net ^{210}Po scavenging processes may be balanced by net regeneration processes within the BNL, or that ^{210}Po processing occurs over a time scale not evidenced within the ^{210}Po lifetime (months). This is consistent with the expected long residence time of the fine suspended particles within BNL. It suggests that ^{210}Po may not be a suitable tracer to quantify the scavenging process occurring in such a BNL.

4.7. Trans-Atlantic Geotraverse (TAG) hydrothermal plume

The TAG hydrothermal plume was encountered between 3170 and 3440 m depth at station USGT11-16. Within the plume, two dissolved samples were collected at 3230 and 3300 m and two particulate samples nearby at 3300 and 3400 m. In comparison to overlying and underlying water, the plume is mainly characterized by an up to three fold increase in small suspended particle mass content and by up to 50 fold increase of the Fe content in the large particle phase, mainly as Fe oxides (i.e., ferrihydrite, Ohnemus and Lam, n.d.).

Mass balance calculations indicate much higher transfer rates of ^{210}Pb from the dissolved to the fine particulate phase inside the plume than outside the plume (Fig. 4). Corresponding residence times of ^{210}Pb in the dissolved phase are 20 ± 8 y, about 5 times lower than outside the plume. This higher transfer rate can be associated with sorption and/or co-precipitation of ^{210}Pb with freshly formed or released small particles (e.g., Fe or Mn oxides) within the plume. However, the ^{210}Pb aggregation and export rates within the plume are not significantly different from rates obtained outside the plume (Fig. 4). Considering the total ^{210}Pb inventory, the residence times with respect to scavenging are similar both within and outside the plume (120 ± 20 y). This is mainly due to the very high ^{210}Pb particulate activities and apparently much longer ^{210}Pb residence times in the particulate phases within the plume than outside the plume (i.e., 62 ± 4 and 1.7 ± 0.3 y in the small and large particulate phases within the plume respectively, while they are 5.5 ± 0.9 and 0.5 ± 0.1 y in the small and large particulate phases outside the plume, respectively). This suggests that the TAG plume acts as a hot spot for dissolved ^{210}Pb removal but not for total ^{210}Pb removal from the water column, likely due to ^{210}Pb accumulation onto small non-settling particles. Scavenging of ^{210}Pb was previously suggested at the Mid-Atlantic Ridge by Bacon et al. (1976), who found anomalously high activities of particulate ^{210}Pb near the Ridge, and this observation is confirmed here. Our results are also in agreement with findings from other hydrothermal areas such as the Juan de Fuca Ridge (Kadko, 1993b), the East Pacific Rise (Kadko et al., 1987) and the Mid-Indian Ridge (Cochran et al., 1983).

In contrast, ^{210}Po does not present a clear trend within the plume, with calculated scavenging rates similar (at 3230 m depth) or slightly higher (at 3300 m depth) to those found outside the plume (Fig. 4). It is thus difficult to conclude if the TAG plume impacts the ^{210}Po behavior. In fact, this pattern reflects the complex ^{210}Po behavior in hydrothermal plumes in agreement with the contrasting results obtained from previous studies. Indeed, several studies reported ^{210}Po deficits (and thus scavenging) in hydrothermal plumes, such as at the East Pacific Rise (Kadko et al., 1987), in the Juan de Fuca Ridge (Hussain et al., 1995) and possibly in hydrothermal waters in the deep Okinawa Trough

Please cite this article as: Rigaud, S., et al., ^{210}Po and ^{210}Pb distribution, dissolved-particulate exchange rates, and particulate export along the North Atlantic US GEOTRACES GA03 section. Deep-Sea Res. II (2015), http://dx.doi.org/10.1016/j.dsr2.2014.11.003

(Nozaki et al., 1990), while Kadko (1993b) reported ^{210}Po equilibrium in most of the stations from the Endeavor Segment and the North Cleft segment of the Juan de Fuca Ridge. Thus in the TAG hydrothermal plume, it is likely that the ^{210}Po scavenging may be locally enhanced (i.e., at 3300 m depth) due to sorption/co-precipitation with freshly formed or released small suspended particles and aggregation into larger settling particles. However, this influence appears relatively low (not seen at 3230 m depth) due to the long residence time of water and small particles in comparison to the short half-life of ^{210}Po. This means that the changes in the vertical dissolved and fine particles profiles of ^{210}Po through the plume are mainly driven by the changes in the ^{210}Pb activity. In contrast, the relatively short residence time of large settling particles (~days) induce the relatively undisturbed ^{210}Po profiles in large particles that linearly increase with depth in the deep water in spite of the presence of the plume (Fig. 3). The observed total ^{210}Po deficit within the TAG plume appears thus to be mainly maintained by the same processes that might lead to the ^{210}Po deficit in other deep waters.

4.8. Comparison with previous datasets from the North Atlantic

In this section, the dataset obtained is compared to those previously published for ^{210}Po and ^{210}Pb dissolved and particulate activities from stations located near those from the GA03 transect (Bacon, 1977; Bacon et al., 1988).

The first study was carried out during the cruise 32 of F. S. "Meteor" in November and December 1973 (Bacon, 1977), that corresponds to a transect in the tropical and eastern North Atlantic with ten stations occupied (Fig. 1): Two located in the western basin, one close to the mid-Atlantic ridge, four in the eastern basin, and two off Portugal. The second study was carried out in July and August 1983 within the SEEP program along the Mid-Atlantic Bight (Bacon et al., 1988), with three stations close to the station USGT11-01 (Fig. 1). These studies both report the distribution of ^{210}Po and ^{210}Pb in the dissolved ($<0.4\,\mu$m) and particulate ($>0.4\,\mu$m) phases. The main differences between these studies and the present one are: (1) the earlier studies used Co-APDC extraction method for the dissolved samples while the present one used $Fe(OH)_3$ extraction method, and (2) the earlier studies collected the particulate samples by onboard filtration with 0.4 μm filters while in the present study, particulate samples were obtained with in situ pumps with 0.8 and 51 μm filters (for small and large particulate fractions respectively, combined here for comparison). Note that in the present study, the particle size between 0.45 and 0.8 μm was thus not collected.

The vertical nuclide profiles obtained along the GA03 transect and the earlier studies are reported for each sub-area (i.e., off the New England Shelf, western basin, Mid-Atlantic Ridge, eastern basin and off Portugal) in Fig. 8. As a whole, the results agree relatively well, and the most general patterns are well conserved. This is especially the case in the eastern basin and near the mid-Atlantic ridge. The higher nuclide activities in the particulate phase and lower activities in the dissolved phase in the hydrothermal plume sampled in station USGT11-16 in this study can be attributed to the more remote location of the station METEOR 18 from the ridge in the earlier study. However, some significant discrepancies between the present and the previous studies appear:

1) The present study reports an about two fold higher dissolved ^{210}Po and ^{210}Pb activities at depth in the western basin. These differences may be attributed to the different geographical location of the stations (i.e., in the tropical North Atlantic for stations METEOR 8 and 12 and in more subtropical latitudes for stations USGT11-10 and USGT11-12; Fig. 1). This suggests different trends in the nuclides distribution over the western basin with latitude.
2) The present study reports higher dissolved ^{210}Po and ^{210}Pb in surface waters, and lower particulate ^{210}Po and higher particulate ^{210}Pb at depth off the New England Shelf. Here one can invoke the potential impact of seasonal variation in local conditions. The SEEP program was carried out in summer under potentially higher productivity conditions (data not available) that may result in higher surface nuclide scavenging and explain the lower dissolved ^{210}Po and ^{210}Pb activity in surface and the higher ^{210}Po activity in the corresponding particulate phase, in comparison to the late fall conditions encountered during the GA03 transect.
3) The present study reports higher dissolved ^{210}Pb at depth off the coast of Portugal. Here, no seasonal or spatial consideration can explain the deviation as the stations considered are very close and occupied during the same season. Such differences may instead be due to variable processes associated with the MOW (see Section 4.5).
4) The ^{210}Pb scavenging rates exhibited strong spatial trends with an increase eastward along the GA03 transect that was not previously reported. This trend is particularly robust as both ^{210}Pb and ^{226}Ra activity profiles had been measured at the same stations along the GA03 transect (Charette, pers. comm.), while they were derived from the Si–^{226}Ra relationship in the previous study (Bacon, 1977). Perhaps this finding demonstrates the importance of measuring all parameters of interest directly, which is achieved within the GEOTRACES program.
5) Finally, the most noted difference between our recent GEOTRACES GA03 results and previous studies concerns the presence or absence of ^{210}Po/^{210}Pb equilibrium in deep water. Bacon (1977) reported a deficit of ^{210}Po in the dissolved phase, but equilibrium when the particulate phase was included. In the current study we reported significant total ^{210}Po deficit in almost all stations at depth. Although we still do not have a clear explanation for this, the number of studies reporting ^{210}Po deficit at depth has increased during the past two decades and tend to indicate that it could be a real and common feature, even in the North Atlantic (see Section 4.3).

5. Conclusion

This study provides the general and detailed distribution of ^{210}Po and ^{210}Pb across dissolved and particulate phases in the North Atlantic along the GA03 GEOTRACES section. It shows that this nuclide pair provides an important metric to assign rates and time scales of biogeochemical scavenging processes both within the ocean and at its interfaces. Firstly, the most general patterns previously described concerning the ^{210}Po and ^{210}Pb distributions in ocean are confirmed. They include (1) total ^{210}Po deficit in surface water and occasional subsurface excess, attributed to biological uptake in surface waters and regeneration in the subsurface, (2) ^{210}Pb excess in the surface due to atmospheric deposition and (3) the ^{210}Pb deficit at depth due to scavenging with settling particles and benthic removal processes.

This study, however, provides several new insights:

- The division of particles into two class sizes reveals that the small particles (0.8–51 μm) generally contain most of the particulate ^{210}Po and ^{210}Pb activities, indicating that the major fluxes, assumed to be associated to large particles ($>51\,\mu$m), is supported by a low fraction of particles. However, the relatively similar vertical profiles of activity in small and large particles suggests strong and relatively rapid interaction (aggregation-disaggregation) between both classes of particles.

Please cite this article as: Rigaud, S., et al., ^{210}Po and ^{210}Pb distribution, dissolved-particulate exchange rates, and particulate export along the North Atlantic US GEOTRACES GA03 section. Deep-Sea Res. II (2015), http://dx.doi.org/10.1016/j.dsr2.2014.11.003

- In the surface, the ^{210}Po scavenging rates and the ^{210}Po activities in large particles were strongly correlated with POC contents in large particles, supporting the role of biogenic particles for ^{210}Po removal from the surface ocean. These correlations, however, were not found in the two stations closest to the coast, perhaps due to different composition and origin of the particulate matter and/or to change over recent time (within months) of the physical and biogeochemical local conditions.
- The surface scavenging of ^{210}Pb was found to be higher close to the ocean margins, but these rates were only approximated in the absence of more comprehensive annual and regional measurements of ^{210}Pb inputs from atmospheric deposition.
- At depth, ^{210}Pb scavenging rates appear to increase with depth and towards the east in the North Atlantic possibly due to the regional contribution of benthic ^{210}Pb scavenging associated with a higher lithogenic particle flux in the eastern basin.
- Results confirmed the presence of total ^{210}Po deficit in deep water that appeared to be, at least in part, related to in situ particle scavenging and to surface productivity.
- In addition, this study revealed specific ^{210}Po and ^{210}Pb distributions and related scavenging processes in turbid environments such as in benthic nepheloid layers (BNL) and the TAG hydrothermal plumes. Both environments clearly enhanced the transfer rates of ^{210}Pb from the dissolved to the particulate phase by increasing the available surface area of particle for ^{210}Pb adsorption. However, the relatively long residence time of small particles in the TAG plume, in which ^{210}Pb is mainly accumulated, does not allow significant total ^{210}Pb removal from the water column. The influence of the BNL and TAG hydrothermal plume on ^{210}Po scavenging appeared to be mainly negligible due to the long residence time of particles in comparison to the even shorter half-life of ^{210}Po.

In the future, the rates obtained here may be used to better understand the dynamic of POC and other particle reactive or bioactive trace elements analyzed during the global GEOTRACES transects, as well as provide future directions for process studies at specific locations in the ocean.

Acknowledgements

We thank the scientists and crew of the R.V. Knorr for their assistance in obtaining our samples during both North Atlantic US GEOTRACES cruises. We particularly acknowledge Chris Hayes and Katharina Pahnke for providing the seawater samples, the members of the pumping team: Paul Morris, Dan Ohnemus, Steven Spike, for providing particulate filters and the ODF team (Mary Johnson, Rob Palomares, Susan Becker, and Courtney Schatzman). Funding for shiptime, sampling operations, and hydrographic data were provided by NSF grants to the US GEOTRACES North Atlantic Transect Management team of W. Jenkins (OCE-0926423), E. Boyle (OCE-0926204), and G. Cutter (OCE-0926092). The National Science Foundation provided support for TC (OCE-0851462), MB (OCE-0851032) and GS (OCE-0960924). GS would like to acknowledge Hiu Yan Choi and Judith Sarkodee-Adoo for help with lab analyses. MB thanks Anupam Kumar for help with the radiochemical work at Wayne State University. The authors also want to acknowledge Bob Anderson, Michiel Rutgers van der Loeff, Kirk Cochran, and one anonymous reviewer for their help in improving this manuscript.

Appendix A

See Table A1.

Table A1
Rigaud et al. (2013), ^{210}Po and ^{210}Pb distribution, dissolved-particulate exchange rates and particulate export along the North Atlantic US GEOTRACES GA03 section.

Dissolved data(< 0.45 μm)								Particulate data															
												Small particles (0.8–51 μm)						Large particles (> 51 μm)					
Station	Sampling date	Lat. (°W)	Long. (°N)	Depth (m)	^{210}Po	±	^{210}Pb	±	Station	Sampling date	Lat. (°W)	Long. (°N)	Depth (m)	^{210}Po	±	^{210}Pb	±	^{210}Po	±	^{210}Pb	±		
					dpm 100 L^{-1}		dpm 100 L^{-1}							dpm 100 L^{-1}		dpm 100 L^{-1}		dpm 100 L^{-1}		dpm 100 L^{-1}			
USGT10-01	17/10/10	9.6604	38.3299	32	3.2	0.6	14.3	1.2	USGT10-01	17/10/10	9.6604	38.3299	30	0.85	0.05	0.78	0.05	0.15	0.01	0.14	0.01		
USGT10-01	17/10/10	9.6604	38.3299	92			8.4	0.8	USGT10-01	17/10/10	9.6604	38.3299	90	0.45	0.03	0.25	0.02	0.05	0.01	0.07	0.01		
USGT10-01	17/10/10	9.6604	38.3299	112	12.5	1.2	6.2	0.6	USGT10-01	17/10/10	9.6604	38.3299	110	0.32	0.02	0.30	0.02	0.06	0.00	0.06	0.00		
USGT10-01	17/10/10	9.6604	38.3299	136	13.8	1.5	10.7	1.1	USGT10-01	17/10/10	9.6604	38.3299	185	0.53	0.03	0.20	0.02	0.04	0.00	0.05	0.00		
USGT10-01	17/10/10	9.6604	38.3299	186	13.5	1.5	12.4	1.1	USGT10-01	17/10/10	9.6604	38.3299	235	0.54	0.03	0.35	0.03	0.03	0.00	0.05	0.01		
USGT10-01	17/10/10	9.6604	38.3299	235			12.3	1.1	USGT10-01	17/10/10	9.6604	38.3299	420	0.85	0.05	0.46	0.04	0.05	0.00	0.05	0.01		
USGT10-01	17/10/10	9.6604	38.3299	418	11.1	1.2	9.7	0.8	USGT10-01	17/10/10	9.6604	38.3299	665	1.09	0.05	0.79	0.05	0.07	0.01	0.16	0.01		
USGT10-01	17/10/10	9.6604	38.3299	660	7.4	1.0	12.3	1.2	USGT10-01	17/10/10	9.6604	38.3299	965	0.92	0.06	0.85	0.05	0.14	0.01	0.21	0.01		
USGT10-01	17/10/10	9.6604	38.3299	957	7.8	0.9	8.2	0.8	USGT10-01	17/10/10	9.6604	38.3299	1200	0.84	0.05	0.78	0.05						
USGT10-01	17/10/10	9.6604	38.3299	1187	4.7	0.8	14.6	1.3	USGT10-01	17/10/10	9.6604	38.3299	1500	0.93	0.05	0.85	0.05						
USGT10-01	17/10/10	9.6604	38.3299	1484	3.6	0.6	9.9	1.1	USGT10-01	17/10/10	9.6604	38.3299	2100	1.19	0.06	0.39	0.03						
USGT10-01	17/10/10	9.6604	38.3299	1781	4.2	0.7	11.3	1.0	USGT10-01	17/10/10	9.6604	38.3299	2700	0.69	0.03	0.47	0.03						
USGT10-01	17/10/10	9.6604	38.3299	2077	4.6	1.1	22.3	1.9	USGT10-09	27/10/10	18.2542	17.3503	26	0.40	0.02	0.27	0.03	0.24	0.01	0.15	0.01		
USGT10-01	17/10/10	9.6604	38.3299	2373	4.7	1.6	19.1	3.6	USGT10-09	27/10/10	18.2542	17.3503	52	0.32	0.02	0.23	0.02	0.12	0.01	0.06	0.01		
USGT10-01	17/10/10	9.6604	38.3299	2670	3.4	0.9	18.3	1.5	USGT10-10	27/10/10	18.2542	17.3503	85	0.31	0.02	0.43	0.03	0.07	0.01	0.08	0.01		
USGT10-01	17/10/10	9.6604	38.3299	2808	2.6	0.7	15.9	1.3	USGT10-11	27/10/10	18.2542	17.3503	135	0.43	0.03	0.44	0.03			0.13	0.01		
USGT10-09	27/10/10	18.2542	17.3503	30	0.00	0.76	22.09	1.65	USGT10-12	27/10/10	18.2542	17.3503	185	0.53	0.03	0.55	0.04	0.08	0.01	0.12	0.01		
USGT10-09	27/10/10	18.2542	17.3503	56	0.00	0.43	8.97	0.75	USGT10-13	27/10/10	18.2542	17.3503	235	0.58	0.03	0.55	0.04	0.08	0.01	0.14	0.01		

Table A1 (*continued*)

Dissolved data(< 0.45 μm)									Particulate data											
														Small particles (0.8–51 μm)				Large particles (> 51 μm)			
Station	Sampling date	Lat. (°W)	Long. (°N)	Depth (m)	^{210}Po	±	^{210}Pb	±	Station	Sampling date	Lat. (°W)	Long. (°N)	Depth (m)	^{210}Po	±	^{210}Pb	±	^{210}Po	±	^{210}Pb	±
					dpm 100 L^{-1}		dpm 100 L^{-1}							dpm 100 L^{-1}		dpm 100 L^{-1}		dpm 100 L^{-1}		dpm 100 L^{-1}	
USGT10-10	27/10/10	18.2542	17.3503	89	5.75	0.79	8.58	0.76	USGT10-14	27/10/10	18.2542	17.3503	390	0.51	0.03	0.41	0.03	0.09	0.01	0.11	0.01
USGT10-11	27/10/10	18.2542	17.3503	138	14.88	1.38	7.12	0.73	USGT10-15	27/10/10	18.2542	17.3503	665	0.66	0.03	0.32	0.02	0.07	0.00	0.05	0.00
USGT10-12	27/10/10	18.2542	17.3503	187	10.20	1.18	10.41	0.94	USGT10-16	27/10/10	18.2542	17.3503	800	0.57	0.03	0.30	0.02	0.06	0.01	0.06	0.00
USGT10-13	27/10/10	18.2542	17.3503	236	9.51	1.08	9.24	0.80	USGT10-17	27/10/10	18.2542	17.3503	950	0.61	0.03	0.31	0.03	0.06	0.00	0.05	0.00
USGT10-14	27/10/10	18.2542	17.3503	389	8.45	1.07	10.73	0.96	USGT10-18	27/10/10	18.2542	17.3503	1250	0.44	0.02	0.40	0.03				
USGT10-15	27/10/10	18.2542	17.3503	662	9.05	0.98	7.03	0.68	USGT10-19	27/10/10	18.2542	17.3503	1700	0.72	0.04	0.41	0.03				
USGT10-16	27/10/10	18.2542	17.3503	957	5.45	0.77	8.97	0.92	USGT10-20	27/10/10	18.2542	17.3503	2100	0.85	0.04	0.35	0.03				
USGT10-17	27/10/10	18.2542	17.3503	1187	2.31	0.92	11.57	1.50	USGT10-21	27/10/10	18.2542	17.3503	2500	1.13	0.06	0.72	0.04				
USGT10-18	27/10/10	18.2542	17.3503	1532	3.58	0.61	8.58	0.78	USGT10-22	27/10/10	18.2542	17.3503	2900	2.34	0.12	2.64	0.15				
USGT10-19	27/10/10	18.2542	17.3503	2075	5.21	0.65	8.29	0.71	USGT10-22	27/10/10	18.2542	17.3503	3000	1.62	0.10	2.52	0.14				
USGT10-20	27/10/10	18.2542	17.3503	2470	4.33	0.65	8.19	0.71	USGT11-01	7/11/11	69.7964	39.6924	30	0.54	0.03	0.35	0.03	0.37	0.02	0.25	0.02
USGT10-21	27/10/10	18.2542	17.3503	2864	1.66	0.25	1.74	0.33	USGT11-01	7/11/11	69.7964	39.6924	58	0.48	0.05	0.99	0.06	0.14	0.01	0.24	0.02
USGT10-22	27/10/10	18.2542	17.3503	3027	2.67	0.31	1.63	0.34	USGT11-01	7/11/11	69.7964	39.6924	90	0.63	0.06	0.92	0.06	0.09	0.01	0.18	0.02
USGT11-01	7/11/11	69.7964	39.6924	30	14.41	1.60	18.60	1.40	USGT11-01	7/11/11	69.7964	39.6924	112	0.64	0.05	0.85	0.05	0.09	0.01	0.18	0.02
USGT11-01	7/11/11	69.7964	39.6924	59	7.37	0.78	7.11	0.64	USGT11-01	7/11/11	69.7964	39.6924	137	0.62	0.05	0.81	0.05	0.13	0.01	0.26	0.02
USGT11-01	7/11/11	69.7964	39.6924	90	9.49	1.04	8.88	0.82	USGT11-01	7/11/11	69.7964	39.6924	186	0.82	0.05	0.72	0.05	0.10	0.01	0.14	0.01
USGT11-01	7/11/11	69.7964	39.6924	111	9.15	0.91	8.80	0.84	USGT11-01	7/11/11	69.7964	39.6924	236	0.87	0.04	0.42	0.03	0.09	0.01	0.11	0.01
USGT11-01	7/11/11	69.7964	39.6924	135	5.53	0.72	11.27	0.89	USGT11-01	7/11/11	69.7964	39.6924	612	0.82	0.04	0.58	0.04	0.09	0.01	0.08	0.01
USGT11-01	7/11/11	69.7964	39.6924	236	4.52	0.75	13.30	1.04	USGT11-01	7/11/11	69.7964	39.6924	912	0.77	0.05	0.56	0.04	0.14	0.01	0.20	0.02
USGT11-01	7/11/11	69.7964	39.6924	420	6.86	0.80	11.28	0.95	USGT11-01	7/11/11	69.7964	39.6924	1147	0.87	0.05	0.58	0.04	0.14	0.01	0.20	0.02
USGT11-01	7/11/11	69.7964	39.6924	599			7.15	0.69	USGT11-01	7/11/11	69.7964	39.6924	1446	0.86	0.05	0.63	0.04	0.18	0.01	0.18	0.01
USGT11-01	7/11/11	69.7964	39.6924	663	6.79	0.76	6.18	0.76	USGT11-01	7/11/11	69.7964	39.6924	1596	0.99	0.06	0.61	0.04	0.21	0.01	0.23	0.02
USGT11-01	7/11/11	69.7964	39.6924	825	4.93	0.70	9.37	0.85	USGT11-01	7/11/11	69.7964	39.6924	1946	1.10	0.05	0.64	0.04	0.32	0.02	0.21	0.02
USGT11-01	7/11/11	69.7964	39.6924	1500	7.25	0.83	8.38	0.76	USGT11-01	7/11/11	69.7964	39.6924	2006	1.21	0.06	0.77	0.05	0.35	0.02	0.29	0.02
USGT11-01	7/11/11	69.7964	39.6924	1798	5.64	0.68	8.74	0.80	USGT11-10	20/11/11	64.1902	31.7368	41	1.08	0.05	0.41	0.03	0.11	0.01	0.09	0.01
USGT11-01	7/11/11	69.7964	39.6924	1998	5.61	0.74	9.27	0.86	USGT11-10	20/11/11	64.1902	31.7368	76	1.00	0.05	0.40	0.04	0.09	0.01	0.07	0.01
USGT11-10	20/11/11	64.1902	31.7368	1	8.32	1.09	17.39	1.47	USGT11-10	20/11/11	64.1902	31.7368	91	0.63	0.04	0.46	0.04	0.07	0.01	0.09	0.01
USGT11-10	20/11/11	64.1902	31.7368	41	6.46	0.95	18.03	1.46	USGT11-10	20/11/11	64.1902	31.7368	111	0.48	0.04	0.37	0.04	0.11	0.01	0.09	0.01
USGT11-10	20/11/11	64.1902	31.7368	75	7.77	0.91	16.81	1.28	USGT11-10	20/11/11	64.1902	31.7368	185	0.29	0.03	0.40	0.03	0.04	0.01	0.09	0.01
USGT11-10	20/11/11	64.1902	31.7368	90	7.93	0.73	13.47	1.10	USGT11-10	20/11/11	64.1902	31.7368	235	0.44	0.03	0.46	0.03	0.05	0.01	0.08	0.01
USGT11-10	20/11/11	64.1902	31.7368	110	14.11	1.36	10.53	0.93	USGT11-10	20/11/11	64.1902	31.7368	417	0.66	0.04	0.57	0.04	0.09	0.01	0.13	0.01
USGT11-10	20/11/11	64.1902	31.7368	185	9.93	0.92	12.32	0.89	USGT11-10	20/11/11	64.1902	31.7368	794	0.77	0.04	0.39	0.03	0.09	0.01	0.06	0.01
USGT11-10	20/11/11	64.1902	31.7368	285	10.64	0.92	14.82	1.07	USGT11-10	20/11/11	64.1902	31.7368	1201	0.77	0.05	0.41	0.03	0.10	0.01	0.07	0.01
USGT11-10	20/11/11	64.1902	31.7368	501	10.99	1.12	13.90	1.10	USGT11-10	20/11/11	64.1902	31.7368	1801	0.99	0.04	0.41	0.03	0.09	0.01	0.05	0.01
USGT11-10	20/11/11	64.1902	31.7368	797	7.10	0.77	9.05	0.72	USGT11-10	20/11/11	64.1902	31.7368	2301	1.11	0.04	0.35	0.03	0.07	0.01	0.04	0.00
USGT11-10	20/11/11	64.1902	31.7368	970	6.11	0.72	8.76	0.78	USGT11-10	20/11/11	64.1902	31.7368	3006	0.87	0.04	0.29	0.02	0.08	0.01	0.03	0.00
USGT11-10	20/11/11	64.1902	31.7368	1497	6.20	0.67	8.00	0.68	USGT11-10	20/11/11	64.1902	31.7368	3603	0.64	0.03	0.26	0.02	0.09	0.01	0.05	0.01
USGT11-10	20/11/11	64.1902	31.7368	2096	7.07	0.71	7.12	0.66	USGT11-10	20/11/11	64.1902	31.7368	3904	0.78	0.04	0.37	0.03	0.06	0.01	0.04	0.00
USGT11-12	24/11/11	56.817	29.7	41	6.97	1.10	23.37	1.70	USGT11-10	20/11/11	64.1902	31.7368	4447	0.96	0.04	0.63	0.04	0.11	0.01	0.11	0.01
USGT11-12	24/11/11	56.817	29.7	100	10.90	1.22	14.91	1.10	USGT11-10	20/11/11	64.1902	31.7368	4492	1.02	0.05	0.67	0.04	0.12	0.01	0.08	0.01
USGT11-12	24/11/11	56.817	29.7	187	10.71	1.12	14.08	1.12	USGT11-12	24/11/11	56.817	29.7	40	2.09	0.08	0.68	0.05	0.12	0.01	0.05	0.01
USGT11-12	24/11/11	56.817	29.7	236	9.81	1.04	13.89	1.04	USGT11-12	24/11/11	56.817	29.7	100	0.51	0.03	0.35	0.03	0.06	0.01	0.04	0.00
USGT11-12	24/11/11	56.817	29.7	287	9.17	0.92	11.95	0.91	USGT11-12	24/11/11	56.817	29.7	185	0.47	0.03	0.48	0.04	0.04	0.01	0.06	0.01
USGT11-12	24/11/11	56.817	29.7	422	9.02	0.99	11.38	0.91	USGT11-12	24/11/11	56.817	29.7	236	0.48	0.03	0.51	0.04	0.06	0.01	0.07	0.01
USGT11-12	24/11/11	56.817	29.7	746	5.92	0.68	9.28	0.74	USGT11-12	24/11/11	56.817	29.7	286	0.44	0.04	0.61	0.04	0.07	0.01	0.08	0.01
USGT11-12	24/11/11	56.817	29.7	999	6.79	0.76	8.77	0.75	USGT11-12	24/11/11	56.817	29.7	420	0.67	0.04	0.50	0.04	0.06	0.01	0.07	0.01
USGT11-12	24/11/11	56.817	29.7	1497	8.49	0.75	4.79	0.48	USGT11-12	24/11/11	56.817	29.7	574	0.71	0.04	0.48	0.04	0.10	0.01	0.07	0.01
USGT11-12	24/11/11	56.817	29.7	2101	7.26	0.76	8.71	0.74	USGT11-12	24/11/11	56.817	29.7	746	0.75	0.03	0.35	0.03	0.07	0.01	0.04	0.00
USGT11-12	24/11/11	56.817	29.7	2997	7.69	0.89	11.57	0.81	USGT11-12	24/11/11	56.817	29.7	1002	0.86	0.04	0.32	0.03	0.07	0.01	0.04	0.00
USGT11-12	24/11/11	56.817	29.7	3893	8.60	0.89	11.69	0.91	USGT11-12	24/11/11	56.817	29.7	1502	0.70	0.04	0.28	0.03	0.06	0.01	0.03	0.00

USGT11-12	24/11/11	56.817	29.7	4689	7.54	0.88	12.24	1.00	USGT11-12	24/11/11	56.817	29.7	2102	0.98	0.05	0.35	0.03	0.05	0.01	0.03	0.00
USGT11-12	24/11/11	56.817	29.7	5088	7.52	0.95	15.05	1.09	USGT11-12	24/11/11	56.817	29.7	3004	1.51	0.06	0.43	0.03	0.15	0.01	0.05	0.01
USGT11-12	24/11/11	56.817	29.7	5467	7.69	0.80	10.78	0.87	USGT11-12	24/11/11	56.817	29.7	3904	1.21	0.05	0.29	0.02	0.12	0.01	0.05	0.01
USGT11-12	24/11/11	56.817	29.7	5604	6.76	0.76	10.50	0.88	USGT11-12	24/11/11	56.817	29.7	4704	1.06	0.06	0.25	0.02	0.08	0.01	0.04	0.00
USGT11-16	29/11/11	44.8262	26.1368	39	8.89	1.26	22.16	1.80	USGT11-12	24/11/11	56.817	29.7	5108	1.47	0.07	0.41	0.03	0.21	0.02	0.08	0.01
USGT11-16	29/11/11	44.8262	26.1368	90	9.59	1.15	17.61	1.34	USGT11-12	24/11/11	56.817	29.7	5485	1.82	0.06	0.48	0.03	0.39	0.02	0.13	0.01
USGT11-16	29/11/11	44.8262	26.1368	114	9.14	1.01	17.11	1.40	USGT11-16	29/11/11	44.8262	26.1368	39	2.88	0.08	0.35	0.03	0.19	0.02	0.07	0.01
USGT11-16	29/11/11	44.8262	26.1368	135	10.90	1.11	15.92	1.28	USGT11-16	29/11/11	44.8262	26.1368	89	0.91	0.04	0.41	0.03	0.13	0.01	0.06	0.01
USGT11-16	29/11/11	44.8262	26.1368	184	9.94	1.10	13.94	1.06	USGT11-16	29/11/11	44.8262	26.1368	114	0.52	0.03	0.46	0.04	0.09	0.01	0.05	0.01
USGT11-16	29/11/11	44.8262	26.1368	234	6.05	0.81	14.93	1.03	USGT11-16	29/11/11	44.8262	26.1368	137	0.40	0.03	0.44	0.03	0.07	0.01	0.08	0.01
USGT11-16	29/11/11	44.8262	26.1368	419	11.80	1.13	8.05	0.72	USGT11-16	29/11/11	44.8262	26.1368	187	0.46	0.03	0.45	0.03	0.09	0.01	0.08	0.01
USGT11-16	29/11/11	44.8262	26.1368	599	9.82	0.97	13.06	1.07	USGT11-16	29/11/11	44.8262	26.1368	237	0.50	0.03	0.40	0.03	0.04	0.01	0.07	0.01
USGT11-16	29/11/11	44.8262	26.1368	801	7.01	0.77	10.39	0.91	USGT11-16	29/11/11	44.8262	26.1368	420	0.70	0.04	0.36	0.03	0.07	0.01	0.04	0.01
USGT11-16	29/11/11	44.8262	26.1368	1497	6.50	0.68	10.37	0.81	USGT11-16	29/11/11	44.8262	26.1368	596	0.81	0.05	0.34	0.03	0.08	0.01	0.04	0.01
USGT11-16	29/11/11	44.8262	26.1368	2088	7.20	0.78	9.09	0.78	USGT11-16	29/11/11	44.8262	26.1368	801	0.60	0.04	0.60	0.04	0.07	0.01	0.04	0.00
USGT11-16	29/11/11	44.8262	26.1368	3228	3.14	0.39	4.76	0.48	USGT11-16	29/11/11	44.8262	26.1368	1501	0.52	0.04	0.34	0.03	0.05	0.01	0.03	0.00
USGT11-16	29/11/11	44.8262	26.1368	3307	1.94	0.41	7.18	0.65	USGT11-16	29/11/11	44.8262	26.1368	2101	1.09	0.05	0.34	0.03	0.06	0.01	0.03	0.00
USGT11-16	29/11/11	44.8262	26.1368	3481	6.78	0.77	9.22	0.77	USGT11-16	29/11/11	44.8262	26.1368	3001	3.52	0.12	1.61	0.09	0.14	0.01	0.09	0.01
USGT11-16	29/11/11	44.8262	26.1368	3606	5.69	0.77	10.94	0.96	USGT11-16	29/11/11	44.8262	26.1368	3301	4.98	0.26	6.80	0.38	0.16	0.02	0.20	0.01
USGT11-20	4/12/11	35.8671	22.333	1	10.11	1.20	17.10	1.36	USGT11-16	29/11/11	44.8262	26.1368	3401	4.20	0.22	5.46	0.31	0.19	0.01	0.13	0.01
USGT11-20	4/12/11	35.8671	22.333	39	5.02	0.76	15.78	1.18	USGT11-16	29/11/11	44.8262	26.1368	3505	2.94	0.11	1.41	0.08	0.18	0.01	0.08	0.01
USGT11-20	4/12/11	35.8671	22.333	74	5.49	0.82	15.01	1.17	USGT11-16	29/11/11	44.8262	26.1368	3600	2.49	0.09	0.71	0.05	0.21	0.01	0.09	0.01
USGT11-20	4/12/11	35.8671	22.333	99	7.50	0.90	14.61	1.17	USGT11-20	4/12/11	35.8671	22.333	40	0.85	0.08	1.65	0.11				
USGT11-20	4/12/11	35.8671	22.333	134	8.02	1.00	16.03	1.28	USGT11-20	4/12/11	35.8671	22.333	75					0.09	0.01	0.05	0.01
USGT11-20	4/12/11	35.8671	22.333	185	10.72	1.01	14.12	1.03	USGT11-20	4/12/11	35.8671	22.333	100	0.63	0.03	0.41	0.03	0.08	0.01	0.04	0.00
USGT11-20	4/12/11	35.8671	22.333	235	9.59	1.00	11.03	0.94	USGT11-20	4/12/11	35.8671	22.333	136	0.42	0.02	0.39	0.03	0.04	0.01	0.06	0.01
USGT11-20	4/12/11	35.8671	22.333	377	6.52	0.77	11.73	0.95	USGT11-20	4/12/11	35.8671	22.333	186	0.39	0.02	0.35	0.03	0.03	0.01	0.07	0.01
USGT11-20	4/12/11	35.8671	22.333	734	7.38	0.82	10.42	0.86	USGT11-20	4/12/11	35.8671	22.333	235					0.04	0.01	0.05	0.01
USGT11-20	4/12/11	35.8671	22.333	1059	10.20	0.93	9.79	0.89	USGT11-20	4/12/11	35.8671	22.333	374	0.50	0.03	0.73	0.05	0.07	0.01	0.05	0.01
USGT11-20	4/12/11	35.8671	22.333	2296	9.02	0.99	12.80	1.03	USGT11-20	4/12/11	35.8671	22.333	732	0.69	0.03	0.24	0.02	0.06	0.01	0.03	0.00
USGT11-20	4/12/11	35.8671	22.333	3492	12.67	1.10	10.73	1.05	USGT11-20	4/12/11	35.8671	22.333	1060	0.70	0.04	0.25	0.02	0.05	0.01	0.04	0.00
USGT11-20	4/12/11	35.8671	22.333	4687	12.59	1.00	11.05	0.88	USGT11-20	4/12/11	35.8671	22.333	2300	1.01	0.06	0.38	0.03	0.07	0.01	0.03	0.00
USGT11-20	4/12/11	35.8671	22.333	5253	10.65	1.09	11.53	1.16	USGT11-20	4/12/11	35.8671	22.333	3500	1.40	0.07	0.34	0.03	0.10	0.01	0.04	0.00
USGT11-20	4/12/11	35.8671	22.333	5302	9.85	1.16	15.52	1.26	USGT11-20	4/12/11	35.8671	22.333	4701	1.64	0.08	0.33	0.03	0.13	0.01	0.05	0.01
USGT11-20	4/12/11	35.8671	22.333	5351	11.28	0.97	7.70	0.67	USGT11-20	4/12/11	35.8671	22.333	5266	2.02	0.10	0.48	0.03	0.18	0.01	0.07	0.01
USGT11-20	4/12/11	35.8671	22.333	5404	14.48	1.40	13.34	0.96	USGT11-20	4/12/11	35.8671	22.333	5316	2.17	0.09	0.49	0.04	0.18	0.01	0.07	0.01
									USGT11-20	4/12/11	35.8671	22.333	5371	2.12	0.10	0.85	0.06	0.19	0.01	0.06	0.01
									USGT11-20	4/12/11	35.8671	22.333	5420	0.47	0.16	4.32	0.28	0.21	0.01	0.06	0.01

Please cite this article as: Rigaud, S., et al., ^{210}Po and ^{210}Pb distribution, dissolved-particulate exchange rates, and particulate export along the North Atlantic US GEOTRACES GA03 section. Deep-Sea Res. II (2015), http://dx.doi.org/10.1016/j.dsr2.2014.11.003

References

Bacon, M.P., 1977. ^{210}Pb and ^{210}Po results from F. S. "Meteor" cruise 32 in the North Atlantic. Meteor Forschungsergebnisse, Dtsch. Forschungsgemeinschaft, R. A Allg. Phys. und Chemie des Meeres, 19. Gebrüder Bornträger, Berlin, Stuttgart, pp. 24–36.

Bacon, M.P., Anderson, F.R., 1982. Distribution of thorium isotopes between dissolved and particulate forms in the deep sea. J. Geophys. Res. 87, 2045–2056.

Bacon, M.P., Belastock, R.A., Tecotzky, M., Turekian, K.K., Spencer, D.W., 1988. Lead-210 and polonium-210 in ocean water profiles of the continental shelf and slope south of New England. Cont. Shelf Res. 8, 841–853.

Bacon, M.P., Brewer, P.G., Spencer, D.W., Murray, J.W., Goddard, J., 1980. Lead-210, polonium-210, manganese and iron in the Cariaco Trench. Deep Sea Res. Part A: Oceanogr. Res. Pap 27, 119–135.

Bacon, M.P., Spencer, D.W., Brewer, P.G., 1976. ^{210}Pb/^{226}Ra and ^{210}Po/^{210}Pb disequilibria in seawater and suspended particulate matter. Earth Planet. Sci. Lett. 32, 277–296.

Bacon, M.P., Spencer, D.W., Brewer, P.G., 1978. Lead-210 and Polonium-210 as Marine Geochemical Tracers: Review and Discussion of Results from the Labrador Sea. In: Gesell, T.F., Lowder, W.F. (Eds.), U.S. Department of Energy Report CONF-780422. Natural Radiation Environment III, Houston, Texas.

Baskaran, M., 2011. Po-210 and Pb-210 as atmospheric tracers and global atmospheric Pb-210 fallout: a review. J. Environ. Radioact. 102, 500–513.

Baskaran, M., Church, T., Hong, G.-H., Kumar, A., Qiang, M., Choi, H.J., Rigaud, S., Maiti, K., 2013. Effects of flow rates and composition of the filter, and decay/ingrowth correction factors involved with the determination of in-situ particulate ^{210}Po and ^{210}Pb in seawater. Limnol. Oceanogr. Methods 11, 126–138.

Benninger, L.K., 1978. 210Pb balance in Long Island Sound. Geochim. Cosmochim. Acta 42, 1165–1174.

Bruland, K.W., Koide, M., Goldberg, E.D., 1974. The comparative marine geochemistries of lead 210 and radium 226. J. Geophys. Res. 79, 3083–3086.

Charette M., Morris P., Henderson P., Moore W. Radium isotope distributions during the US GEOTRACES North Atlantic Cruises. Mar. Chem. (in press).

Chung, Y., 1987. ^{210}Pb in the western Indian Ocean: distribution, disequilibrium, and partitioning between dissolved and particulate phases. Earth Planet. Sci. Lett 85, 28–40.

Chung, Y., Finkel, R., 1988. 210Po in the western Indian Ocean: distributions, disequilibria and partitioning between the dissolved and particulate phases. Earth Planet. Sci. Lett. 88, 232–240.

Chung, Y., Wu, T., 2005. Large ^{210}Po deficiency in the northern South China Sea. Cont. Shelf Res. 25, 1209–1224.

Church, T., Rigaud, S., Baskaran, M., Kumar, A., Friedrich, J., Masque, P., Puigcorbé, V., Kim, G., Radakovitch, O., Hong, G., 2012. Intercalibration studies of ^{210}Po and ^{210}Pb in dissolved and particulate seawater samples. Limnol. Oceanogr. Methods 10, 776–789. http://dx.doi.org/10.4319/lom.2012.10.776.

Clegg, S.L., Whitfield, M., 1991. A generalized model for the scavenging of trace metals in the open ocean—II. Thorium scavenging. Deep Sea Res. Part A: Oceanogr. Res. Pap 38, 91–120.

Cochran, J.K., 1992. The oceanic chemistry of the uranium- and thorium-series nuclides. In: Ivanovich, M., Harmon, R.S.Please confirm that given names and surnames have been identified correctly for authors. (Eds.), Uranium-Series Disequilibrium—Applications to Earth, Marine, and Environmental Sciences. U. Clarendon Press, Oxford, pp. 334–395.

Cochran, J.K., Bacon, M.P., Krishnaswami, S., Turekian, K.K., 1983. 210Po and 210Pb distributions in the central and eastern Indian Ocean. Earth Planet. Sci. Lett. 65, 433–452.

Cochran, J.K., Masque, P., 2003. Short-lived U/Th series radionuclides in the ocean: tracers for scavenging rates, export fluxes and particle dynamics. In: Bourdon, B.P., Henderson, G., Lundstrom, C.C., Turner, S.P. (Eds.), Uranium Series Geochemistry. Reviews in Mineralogy and Geochemistry. Mineralogical Society of America, pp. 461–492.

Cochran, J.K., McKibbin-Vaughan, T., Dornblaser, M.M., Hirschberg, D., Livingston, H. D., Buesseler, K.O., 1990. 210Pb scavenging in the North Atlantic and North Pacific Oceans. Earth Planet. Sci. Lett. 97, 332–352.

Craig, H., Krishnaswami, S., Somayajulu, B.L.K., 1973. ^{210}Pb–^{226}Ra: Radioactive disequilibrium in the deep sea . Earth Planet. Sci. Lett. 17, 295–305.

Flynn, W.W., 1968. The determination of low levels of polonium-210 in environmental materials. Anal. Chim. Acta 43, 221–227.

Friedrich, J., Rutgers van der Loeff, M.M., 2002. A two-tracer (^{210}Po–^{234}Th) approach to distinguish organic carbon and biogenic silica export flux in the Antarctic Circumpolar Current. Deep Sea Res. Part I: Oceanogr. Res. Pap 49, 101–120.

Gascó, C., Antón, M.P., Delfanti, R., González, A.M., Meral, J., Papucci, C., 2002. Variation of the activity concentrations and fluxes of natural (^{210}Po, ^{210}Pb) and anthropogenic (^{239,240}Pu, ^{137}Cs) radionuclides in the Strait of Gibraltar (Spain). J. Environ. Radioact. 62, 241–262.

Hartman, M.C., 1987. The Total Deposition of Pb, Cd, Zn and 210Pb and Atmospheric Transport to the Western Atlantic Using ^{222}Rn and Air Mass Trajectory Analysis. University of Delaware.

Hatta, M., Measures, C.I., Wu, J., Fitzsimmons, J., Sedgwick, P., Morton, P., Overview: Dissolved Fe and Mn concentrations in the North Atlantic Ocean during GEOTRACES 2010/2011 cruises. Deep-Sea Res. II, this issue [http://dx.doi.org/10.1016/j.dsr2.2014.07.005].

Henderson, G.M., Maier-Reimer, E., 2002. Advection and removal of ^{210}Pb and stable Pb isotopes in the oceans: a general circulation model study. Geochim. Cosmochim. Acta 66, 257–272.

Hong, G.H., Baskaran, M., Church, T.M., Conte, M., 2013. Scavenging, cycling and removal fluxes of ^{210}Po and ^{210}Pb at the Bermuda time-series study site. Deep Sea Res. Part II: Top. Stud. Oceanogr 93, 108–118.

Hu, W., Chen, M., Yang, W., Zhang, R., Qiu, Y., Zheng, M., 2014. Enhanced particle scavenging in deep water of the Aleutian Basin revealed by ^{210}Po–^{210}Pb disequilibria. J. Geophys. Res. Ocean, 1–14. http://dx.doi.org/10.1002/2014JC009819.Received.

Heyraud, M., Cherry, R.D., 1979. Polonium-210 and lead-210 in marine food chains. Mar. Biol. 52, 227–236. http://dx.doi.org/10.1007/BF00398136.

Hussain, N., Church, T.M., Luther III, G.W., Moore, W.S., 1995. ^{210}Po and ^{210}Pb disequilibrium in the hydrothermal vent fluids and chimney deposits from Juan de Fuca Ridge. Geophys. Res. Lett. 22, 3175–3178.

Jenkins, W.J., Smethie, W.M., Boyle, E.A., Cutter, G.C., Water mass analysis for the U. S. GEOTRACES North Atlantic sections. Deep-Sea Res. II, this issue [http://dx.doi.org/10.1016/j.dsr2.2014.11.018].

Kadko, D., 1993a. Excess ^{210}Po and nutrient recycling within the California Coastal Transition Zone. J. Geophys. Res. 98, 857–864.

Kadko, D., 1993b. An assessment of the effect of chemical scavenging within submarine hydrothermal plumes upon ocean geochemistry. Earth Planet. Sci. Lett. 120, 361–374.

Kadko, D., Bacon, M.P., Hudson, A., 1987. Enhanced scavenging of ^{210}Pb and ^{210}Po by processes associated with the East Pacific Rise near 8°45′N. Earth Planet. Sci. Lett. 81, 349–357.

Kim, G., 2001. Large deficiency of polonium in the oligotrophic ocean's interior. Earth Planet. Sci. Lett. 192, 15–21.

Kim, G., Alleman, L., Church, T., 1999. Atmospheric depositional fluxes of trace elements, ^{210}Pb, and ^{7}Be to the Sargasso Sea. Global Biogeochem. Cycles 13, 1183–1192.

Kim, G., Church, T., 2001. Seasonal biogeochemical fluxes of 234Th and210Po in the Upper Sargasso Sea: influence from atmospheric iron deposition. Global Biogeochem. Cycles 15, 651–661.

Lam, P.J., Ohnemus, Auro, M.E., Size-fractionated major particle composition and concentrations from the USGEOTRACES North Atlantic Zonal Transect . Deep-Sea Res. II, this issue [http://dx.doi.org/10.1016/j.dsr2.2014.11.020].

Lozano, R.L., Hernández-Ceballos, M.a., Rodrigo, J.F., San Miguel, E.G., Casas-Ruiz, M., García-Tenorio, R., Bolívar, J.P., 2013. Mesoscale behavior of ^{7}Be and ^{210}Pb in superficial air along the Gulf of Cadiz (South of Iberian Peninsula). Atmos. Environ. 80, 75–84. http://dx.doi.org/10.1016/j.atmosenv.2013.07.050.

Measures, C.I., Hatta, M., Fitzsimmons, J., Morton, P., Dissolved Al in the zonal N Atlantic section of the US GEOTRACES 2010/2011 cruises. Deep-Sea Res. II, this issue [http://dx.doi.org/10.1016/j.dsr2.2014.07.006].

Miralles, J., Radakovitch, O., Aloisi, J.-C., 2005. 210Pb sedimentation rates from the Northwestern Mediterranean margin. Mar. Geol 216, 155–167. http://dx.doi.org/10.1016/j.margeo.2005.02.020.

Murray, J.W., Paul, B., Dunne, J.P., Chapin, T., 2005. ^{234}Th, ^{210}Pb, ^{210}Po and stable Pb in the central equatorial Pacific: tracers for particle cycling. Deep Sea Res. Part I: Oceanogr. Res. Pap 52, 2109–2139. http://dx.doi.org/10.1016/j.dsr.2005.06.016.

Noble, A.E., Echegoyen-Sanz, Y., Boyle, E.A., Ohnemus, D.C., Lam, P.J., Kayser, R., Reuer, M., Wu, J., Smethie, W. Dynamic variability of dissolved Pb and Pb isotope composition from the U.S. North Atlantic GEOTRACES Transect. Deep Sea Res. II, http://dx.doi.org/10.1016/j.dsr2.2014.11.011, this issue.

Nozaki, Y., Ikuta, N., Yashima, M., 1990. Unusually large ^{210}Po deficiencies relative to ^{210}Pb in the Kuroshio current of the East China and Philippine seas. J. Geophys. Res. Ocean 95, 5321–5329. http://dx.doi.org/10.1029/JC095iC04p05321.

Nozaki, Y., Thomson, J., Turekian, K.K., 1976. The distribution of ^{210}Pb and ^{210}Po in the surface waters of the Pacific Ocean. Earth Planet. Sci. Lett. 32, 304–312.

Ohnemus, D.C., Lam, P.J., Cycling of lithogenic marine particulates in the US GEOTRACES North Atlantic transect. Deep-Sea Res. II, this issue [http://dx.doi.org/10.1016/j.dsr2.2014.11.019].

Preiss, N., Genthon, C., 1997. Use of a new database of lead 210 for global aerosol model validation. J. Geophys. Res. 102, 347–357.

Renfro, A.A., Cochran, J.K., Colle, B.A., 2013. Atmospheric fluxes of ^{7}Be and ^{210}Pb on monthly time-scales and during rainfall events at Stony Brook, New York (USA). J. Environ. Radioact. 116, 114–123.

Rigaud, S., Puigcorbé, V., Cámara-Mor, P., Casacuberta, N., Roca-Martí, M., Garcia-Orellana, J., Benitez-Nelson, C.R., Masqué, P., Church, T., 2013. A methods assessment and recommendations for improving calculations and reducing uncertainties in the determination of ^{210}Po and ^{210}Pb activities in sea water. Limnol. Oceanogr. Methods 11, 561–571. http://dx.doi.org/10.4319/lom.2013.11.561.

Rutgers van der Loeff, M.M., Geibert, W., 2008. U- and Th-series nuclides as tracers of particle dynamics, scavenging and biogeochemical cycles in the Oceans. In: Krishnaswami, J.K., Cochran, J.K. (Eds.), Radioactivity in the Environment. Elsevier, pp. 227–268.

Sarin, M.M., Krishnaswami, S., Ramesh, R., Somayajulu, B.L.K., 1994. ^{238}U decay series nuclides in the northeastern Arabian Sea: scavenging rates and cycling processes. Cont. Shelf Res. 14, 251–265. http://dx.doi.org/10.1016/0278-4343(94)90015-9.

Schmidt, S., 2006. Impact of the Mediterranean outflow water on particle dynamics in intermediate waters of the Northeast Atlantic, as revealed by ^{234}Th and ^{228}Th. Mar. Chem. 100, 289–298.

Shimmield, G.B., Ritchie, G.D., Fileman, T.W., 1995. The impact of marginal sea zone processes on the distribution of ^{210}Pb, ^{210}Po and ^{234}Th and implications for new production in the Bellinghausen Sea, Antarctica. Deep Sea Res. II 42, 1313–1335.

Spencer, D.W., Bacon, M.P., Brewer, P.G., 1981. Models of the distribution of ^{210}Pb in a section across the North Equatorial Atlantic Ocean. J. Mar. Res. 39, 119–138.

Please cite this article as: Rigaud, S., et al., ^{210}Po and ^{210}Pb distribution, dissolved-particulate exchange rates, and particulate export along the North Atlantic US GEOTRACES GA03 section. Deep-Sea Res. II (2015), http://dx.doi.org/10.1016/j.dsr2.2014.11.003

Stewart, G., Kirk Cochran, J., Xue, J., Lee, C., Wakeham, S.G., Armstrong, R.A., Masqué, P., Carlos Miquel, J., 2007. Exploring the connection between ^{210}Po and organic matter in the northwestern Mediterranean. Deep Sea Res. Part I: Oceanogr. Res. Pap 54, 415–427.

Stewart, G.M., Bradley Moran, S., Lomas, M.W., 2010. Seasonal POC fluxes at BATS estimated from ^{210}Po deficits. Deep Sea Res. Part I: Oceanogr. Res. Pap 57, 113–124. http://dx.doi.org/10.1016/j.dsr.2009.09.007.

Stewart, G.M., Fisher, N.S., 2003a. Bioaccumulation of polonium-210 in marine copepods. Limnol. Oceanogr. 48, 2011–2019.

Stewart, G.M., Fisher, N.S., 2003b. Experimental studies on the accumulation of polonium-210 by marine phytoplankton. Limnol. Oceanogr 48, 9.

Stewart, G.M., Fowler, S.W., Teyssie, J.-L., Cotret, O., Cochran, J.K., Fisher, N.S., 2005. Contrasting transfer of polonium-210 and lead-210 across three trophic levels in marine plankton. Mar. Ecol. Prog. Ser. 290, 7.

Thomson, J., Turekian, K.K., 1976. 210Po and 210Pb distributions in ocean water profiles from the Eastern South Pacific. Earth Planet. Sci. Lett. 32, 297–303.

Thorpe, S.A., 1976. Variability of the mediterranean undercurrent in the Gulf of Cadiz. Deep Sea Res. Oceanogr. Abstr 23, 711–727.

Todd, J.F., Wong, G.T.F., Olsen, C.R., Larsen, I.L., 1989. Atmospheric depositional characteristics of beryllium 7 and lead 210 along the Southeastern Virginia coast. J. Chim. Phys. Phys.-Chim. Biol 94, 11106–11116.

Turekian, K.K., Benninger, L.K., Dion, E.P., 1983. ^{7}Be and ^{210}Pb total deposition fluxes at New Haven, Connecticut and at Bermuda. J. Geophys. Res. 88, 5411–5415.

Turekian, K.K., Nozaki, Y., 1980. ^{210}Po and ^{210}Pb in the Eastern South Pacific—the role of upwelling on their distributions in the water column. In: Saruhashi, K. (Ed.), 1980. Isotope Marine Chemistry, pp. 157–164.

Turekian, K.K., Nozaki, Y., Benninger, L.K., 1977. Geochemistry of atmospheric radon and radon products. Annu. Rev. Earth Planet. Sci. 5, 227–255.

Verdeny, E., Masqué, P., Garcia-Orellana, J., Hanfland, C., Kirk Cochran, J., Stewart, G. M., 2009. POC export from ocean surface waters by means of ^{234}Th/^{238}U and ^{210}Po/^{210}Pb disequilibria: a review of the use of two radiotracer pairs. Deep Sea Res. Part II: Top. Stud. Oceanogr 56, 1502–1518. http://dx.doi.org/10.1016/j.dsr2.2008.12.018.

Verdeny, E., Masqué, P., Maiti, K., Garcia-Orellana, J., Bruach, J.M., Mahaffey, C., Benitez-Nelson, C.R., 2008. Particle export within cyclonic Hawaiian lee eddies derived from ^{210}Pb–^{210}Po disequilibrium. Deep Sea Res. Part II: Top. Stud. Oceanogr 55, 1461–1472. http://dx.doi.org/10.1016/j.dsr2.2008.02.009.

Yang, W.F., Huang, Y.P., Chen, M., Qiu, Y.S., Li, H.B., Zhang, L., 2011. Carbon and nitrogen cycling in the Zhubi coral reef lagoon of the South China Sea as revealed by ^{210}Po and ^{210}Pb. Mar. Pollut. Bull. 62, 905–911.

Please cite this article as: Rigaud, S., et al., ^{210}Po and ^{210}Pb distribution, dissolved-particulate exchange rates, and particulate export along the North Atlantic US GEOTRACES GA03 section. Deep-Sea Res. II (2015), http://dx.doi.org/10.1016/j.dsr2.2014.11.003